Chapter 3 Planets In The South: Astrometric Search For Companions To Stars On The University Of Virginia Southern Parallax Program

3.1 INTRODUCTION

Although the presence of planets orbiting Barnard's Star described by van de Kamp (1963b, 1982) remains unconfirmed, an increasing number of extrasolar planets are being detected and confirmed. As of 2006 August 28, the International Astronomical Union (IAU) Working Group (WG) on Extrasolar Planets (ESP) listed 176 planets orbiting main sequence stars.[7] Marcy *et al*. (2005) estimate that 12 percent (%) of stars host at least one giant planet within 20 astronomical units (AU) based on their radial-velocity studies of 1,330 F, G, K, and M stars with multiple planets in approximately 1% of those systems. This detection rate suggests that as many as eleven stars out of the approximately ninety stars observed in the University of Virginia (UVa) Southern Parallax Program (SPP) might have a planet. The subsample of thirteen stars studied herein might be expected to host up to two planets. However, Butler *et al.* (2004) have detected fewer than expected giant planets orbiting M dwarfs. Because radial-velocity programs have only studied a small sample of such cool stars so far, Endl *et al*. (2003) have begun a program focused on these late types.

Although a wealth of information about extrasolar planets may be obtained by an astrometric planet search, the SPP was not designed specifically for those goals. The SPP sought to identify new stellar members of the solar neighborhood. However, having measured the parallaxes and proper motions of possible nearby stars, the

[7]The IAU WG ESP maintains a list of extrasolar planets at http://www.dtm.ciw.edu/boss/planets.html

analysis of the residuals from the parallax solutions for any periodic perturbations that might indicate unseen companions is a reasonable extension of the program. Because these stars have low masses, their reflex displacement will be greater. Also, because these stars are close, the angular size of that displacement will be more easily detected. Sozzetti (2005) discusses the corresponding astrometric signature (α_{sig} in seconds of arc)

$$\alpha_{sig} = \frac{M_p}{M_*}\frac{a}{d} \tag{3.1}$$

at length, where M_p and M_* are the masses of the planet and its host, respectively, in solar mass units, a is the semi-major axis in AU, and d is the distance in parsecs. The detection or non-detection of such planets would provide additional insight into the frequency of planets around low mass stars. Until recently, all very low luminosity stars were found through their associated astrometric perturbations, mostly at Sproul Observatory (Lippincott 1978). Therefore, the detection of any companions, regardless of mass, would be of scientific significance and improve our knowledge multiplicity within the solar neighborhood.

3.2 MEASUREMENT AND ANALYSIS

The SPP observed approximately ninety stars from 1987 until 2002 using the 1-meter reflector at Siding Springs Observatory, which is described in Table 3.1. Over the course of observations, several different charge-coupled device (CCD's) detectors were used with the 1-meter reflector. Of these, the two used primarily were CCD #1 and CCD #6; only images taken with either of these were considered for astrometric reduction. The first, GEC P8603 EEV, operated from 1987 through early 1994. Its

replacement, a GEC P88500, functioned from 1994 until the end of the project in 2002. Table 3.2 details the two astrometric detectors. Observations were made through the V_C, R_C, and I_C filters (M. Bessell 1999, private communication) specified in Table 3.3. Begam, Ianna, and Patterson (2006, in preparation; hereafter BIP) provide additional details of the SPP.

TABLE 3.1
CHARACTERISTICS OF THE SIDING SPRING REFLECTOR

Parameter		Description
Objective Size	(meter)	1
	(inches)	40
Optics		Ritchey-Chrétien
Focal Ratio		f/8
Focal Length	(meters)	~8.1
Focal Plane Scale (" mm^{-1})		25.55

NOTE.—Table 3.2 details the CCD's used with this telescope. Table 3.3 describes the filters.
REFERENCES.—Patterson, Ianna, & Begam 1998; BIP; MSSSO 2006[8]

TABLE 3.2
CHARACTERISTICS OF CCD'S USED

Parameter	CCD #1	CCD #6
Dates	1987 Jul—1994 Feb	1994 Jan—2002 Jul
Chip	GEC P8603 EEV	GEC P88500 EEV
Size (pixels)	380 x 578	2186 x 1152
CCD Pixel Size (μm)	22.0	22.5
CCD resolution (" $pixel^{-1}$)	0.5621	0.5749
Description	thick, front-illuminated	thick, front-illuminated, uncoated
Grade	A	Engineering

REFERENCES.—RSAA Detector Lab. 2006[9]; M. Begam 2006, private communication; BIP

[8]Mount Stromlo and Siding Spring Observatories maintain a telescope specifications on-line at http://www.mso.anu.edu.au/observing/telescopes/40inch.php
[9]Details of various CCD's maintained by the Research School of Astronomy and Astrophysics Detector Laboratory may be found at http://www.mso.anu.edu.au/observing/detectors/ccdlab/ccdinstr/ccdinstr.htm

TABLE 3.3
CHARACTERISTICS OF FILTERS USED

Filter (Cousins)	Passband (nanometers)	Effective Wavelength (nanometers)
V	470.00 – 650.00	551.28
R	550.00 – 880.00	654.82
I	690.00 – 1,060.00	816.10

REFERENCE.—M. Bessell 1999, private communication

The use of CCD's to record the images of stars by the SPP, rather than photographic plates as was used to record images of Barnard's Star, is especially appropriate for low mass stars. The quantum efficiency of CCD's can reach 90% for wavelengths close to 750 nanometers (nm) compared with about 1% for photographic emulsions (Kitchen 1998). The greater sensitivity of CCD's to longer wavelengths of light is better than photographic plates for the many M dwarfs that the SPP observed and for the filters employed. In addition, CCD's have a greater dynamic range than photographic plates. Because of their low noise, CCD's can reach a similar signal-to-noise ratio 20–30 times faster than a photographic plate (Kitchen 1998). However, photographic plates have the advantage of a longer stable life. Eastman Kodak 103a-G photographic plates were used to image Barnard's Star for over twenty-nine years while multiple CCD's were used with the Siding Spring reflector during the fifteen years of SPP operations.

From the overall SPP program, eight stars, with spectral types from early to middle M that lie between 3.5 and 22 parsecs (pc) away, were initially selected for time series analysis. The stars in this first subsample were observed at least eighty-one times over a minimum of two years; in most cases, observations continued after the selection

of this subsample. The longest baseline for any of these stars was 8.2 years. The resulting errors in the relative parallaxes calculated for these stars are less than 3 mas. This subsample was the subject of a preliminary analysis using the McCormick Parallax Reduction Program (sager; hereinafter MPRP), which is discussed by Bartlett, Ianna, and Begam (2002). The preliminary periodograms produced no clear indication of unseen companions, but those for LHS 288 and LHS 2813 displayed some interesting features, as illustrated in Figure 3.1.

The especially noisy periodograms calculated for LHS 288 led to a complete re-reduction of this field. For some fields, additional observations became available after the preliminary analysis.After the SPP concluded operations, an additional five stars were selected based on the quality of their parallax solutions. The single stars in this second subsample were observed at least fifteen times over a minimum of five years also producing a relative parallax with an error of 3 mas or less. These stars, which lie between 6.5 and 22 pc, also have spectral types between early and middle M plus one white dwarf. Table 3.4 and Table 3.5 describe the selected stars. The SPP previously published photometry for LHS 337 and LHS 532, which can be found in Table 3.6.

Selecting stars based on the quality of their parallax solution can be approached in one of two ways. As done here, potential hosts may be selected for small errors associated with their final parallax that should be accompanied by small residuals. A perturbation due to a companion should stand out from the noise in the

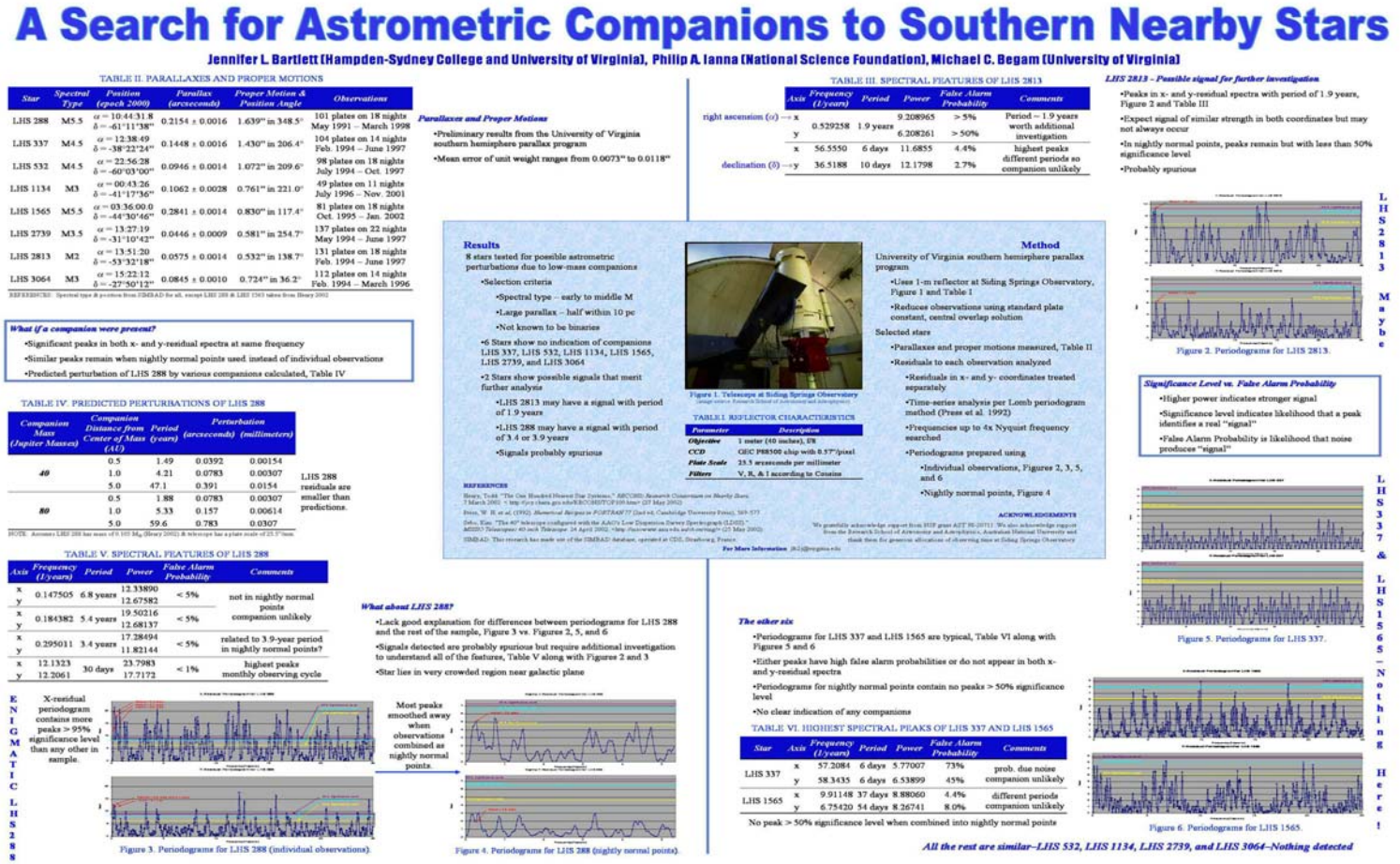

FIG. 3.1.— Summary of Results from the Preliminary Analysis (Bartlett, Ianna, & Begam 2002).

TABLE 3.4
POTENTIAL HOST STARS FROM THE SPP

Star (LHS)	Position (2000.0)[a] RA (hh mm ss.ss)	Dec (dd mm ss.s)	Spectral Type	Apparent Visual Magnitude[b]	Sample[c]	References
34	07 53 08.16	-67 47 31.5	DQ9	13.6 ± 0.3	2	1, 2
271	09 42 46.36	-68 53 06.1	M4.5 V	12.72 ± 0.03	2	3, 4
288	10 44 21.24	-61 12 35.6	M5.5 V	13.90 ± 0.03	1	5, 4
337	12 38 49.10	-38 22 53.7	M4.5 V	12.78 ± 0.05	1	6, 7
532	22 56 24.66	-60 03 49.2	M5.0 V	14.01 ± 0.05	1+	4, 7
1134	00 43 26.01	-41 17 34.0	M3.0 V	13.1[d] ± 0.4[e]	1+	6, 8
1565	03 35 59.72	-44 30 45.5	M5.5 V	13.03 ± 0.01[f]	1	9, 10
2310	10 47 38.69	-79 27 45.9	M3.0 V	13.45 ± 0.01[f]	2	6, 11
2739	13 27 19.59	-31 10 39.7	M3.5 V	13.58 ± 0.015	1+	6, 12
2813	13 51 21.75	-53 32 46.0	M2.0 V	12.9 ± 0.01[f]	1+	6, 11
3064	15 22 12.98	-27 49 42.7	M3:	13.28 ± 0.01[f]	1+	13, 14
3242	16 48 24.49	-72 58 34.1	M0.5 V	11.44 ± 0.01	2	6, 15
3418	18 52 00.17	-60 46 11.3	M3.5 V	13.4[d] ± 0.4[e]	2	6, 9

NOTES.— [a]Coordinates from 2MASS were updated with preliminary relative proper motions from BIP using addpm routine from Jao 2004

[b]Apparent visual magnitude on the Johnson-Morgan system (16, 17) with V=550 nm; $V_{Cousins}$, V_{Kron}, and V_{Eggen} are substantially the same according to 18 and are used here where appropriate

[c]Plus (+) in this column indicates that additional frames became available after the initial analysis of this star as part of sample 1

[d]Assumed to be Johnson-Morgan V-band magnitude

[e]Photometric error estimated from quality of reported absolute V magnitude

[f]Photometric error estimated from 19

REFERENCES.—(1) McCook & Sion 2003; (2) Bessell 1990; (3) Henry *et al*. 2002; (4) Henry *et al*. 2004; (5) Bessell 1991; (6) Hawley, Gizis, & Reid 1996; (7) Patterson, Ianna, & Begam 1998; (8) Gliese & Jahreiß 1991; (9) Henry *et al*. 1997; (10) Rodgers & Eggen 1974; (11) Eggen 1987; (12) Reid, Kilkenny, & Cruz 2002; (13) Bidelman 1985; (14) Eggen 1969; (15) ESA 1997; (16) Johnson & Morgan 1951; (17) Johnson & Morgan 1953; (18) Bessell and Weis 1987; (19) Ryan 1989

TABLE 3.5
PRELIMINARY RELATIVE PARALLAXES AND PROPER MOTIONS FROM THE SPP

Star (LHS)	Parallax (mas)	Proper Motion (mas year^{-1})	Position Angle (degrees)	Mean Error[a] (μm) X	Y	Observations Images	Nights	Start	Stop
34	117.9 ± 1.8	2102.65 ± 0.70	135.804 ± 0.019	0.38	0.38	106	23	1995 Feb	2001 Dec
271	153.8 ± 1.4	1118.51 ± 0.60	356.160 ± 0.015	0.39	0.75	131	27	1992 Jan	2002 Jan
288	213.4 ± 1.7	1641.99 ± 0.61	348.513 ± 0.028	0.54	0.37	105	18	1991 May	1998 Mar
337	145.9 ± 1.4	1432.30 ± 0.86	206.375 ± 0.030	0.33	0.43	104	14	1994 Feb	1997 Jun
532	94.2 ± 1.4	1074.27 ± 0.70	209.672 ± 0.037	0.37	0.36	101[b]	20	1994 Jul	2001 Aug
1134	99.2 ± 2.2	764.55 ± 0.70	221.001 ± 0.052	0.33	0.42	51	12	1996 Jul	2002 Jun
1565	284.5 ± 1.4	830.83 ± 0.45	117.404 ± 0.039	0.29	0.46	81	18	1995 Oct	2002 Jan
2310	71.1 ± 2.8	483.62 ± 0.95	244.224 ± 0.091	0.56	0.58	114[b]	20	1994 Apr	2001 Jan
2739	43.6 ± 0.9	581.37 ± 0.50	254.639 ± 0.049	0.3	0.31	141[b]	24	1994 Apr	2001 Jun
2813	59.8 ± 1.7	533.70 ± 0.60	138.608 ± 0.064	0.51	0.45	136	19	1994 Feb	2002 Apr
3064	82.7 ± 1.0	729.00 ± 0.47	36.117 ± 0.034	0.31	0.37	121	16	1994 Feb	2002 Apr
3242	64.6 ± 1.3	712.49 ± 0.66	222.429 ± 0.052	0.39	0.45	127	20	1994 Feb	2001 May
3418	45.2 ± 0.9	724.82 ± 0.42	298.064 ± 0.038	0.27	0.33	123	20	1994 Apr	2000 Sep

NOTES.— [a]Mean error of unit weight

[b]One questionable image was used in calculating positions and motions of reference stars only. This frame was dropped from the relative parallax and proper motion calculation and did not produce residuals. Therefore, the time-series analysis considered one residual fewer.

REFERENCE.—BIP

TABLE 3.6
SPP PHOTOMETRY OF POTENTIAL HOST STARS

Star (LHS)	V_C (mag)	R_C (mag)	I_C (mag)
337	12.78 ± 0.05	11.48 ± 0.06	9.75 ± 0.06
532	14.01 ± 0.05	12.50 ± 0.06	10.75 ± 0.06

REFERENCE.—Patterson, Ianna, & Begam 1998

residuals. On the other hand, the small errors may be an indication that no orbital component is present. In the alternative approach, larger errors may identify host candidates. The correspondinglarge residuals may be evidence of the presence of an orbital component. The large error, however, may merely reflect noisy or sparse data. In this study, we selected candidate hosts with "clean" parallaxes in the hopes of finding clear evidence of companions.

The observations for each star in this study were made over only a few years; for LHS 271 with the longest baseline, images were taken over 10 years. Therefore, annual normal points were not considered. The results for each individual star are discussed below.The reference stars relative to which the parallax and proper motion of the possible nearby star of interest were measured were selected so that they surrounded the star of interest and shared a common apparent brightness with it. Potential reference stars that were identifiable close binaries were excluded. However, the colors are rarely identical and, consequently, their apparent positions change slightly relative to one another as the atmosphere refracts their light differently as a function of hour angle. Such differential color refraction (DCR) may be minimized by restricting analysis of frames to images taken within 30 minutes of the transit. However, observational circumstances may require the consideration of frames taken at somewhat larger hour

angles; Table 3.7 lists the number of frames used for each star that were taken either 30 minutes or more east or west of the meridian. When possible, the SPP used photometry and weather records to model and correct the positions of stellar images for DCR before the calculation of parallaxes and proper motions. BIP discusses the approach used to model DCR, which is essentially that of Stone (1996). Table 3.7 also provides the status of DCR corrections for the stars in this study.

TABLE 3.7
DCR CORRECTION STATUS FOR SPP STARS

Star (LHS)	Filter (Cousins)	Large HA (# frames)	DCR Status	Comment
34	I	6	Uncorrected	unreduced I and R photometry exists
271	R	24	Uncorrected	no photometry exists
288	R	19	Corrected	
337	R	16	Corrected	
532	R	9	Corrected	
1134	R	5	Uncorrected	unreduced photometry exists
1565	V	4	Uncorrected	unreduced photometry exists
2310	R	9	Uncorrected	no photometry exists
2739	R	10	Corrected	photometry missing for 3/14 ref. stars weather missing for 30/141 frames
2813	R	27	Corrected	
3064	R	17	Corrected	
3242	V	3	Uncorrected	current photometry inadequate
3418	R	20	Corrected	

NOTE.—An exposure is considered to have a large hour angle (HA) if it was taken at 30 minutes or more east or west of the meridian.
REFERENCE.—BIP

The MPRP, the least-squares adjustment program that was used for the study of Barnard's Star and for the preliminary analysis, was designed for photographic plates scanned by a Photometric Data Systems (PDS) microdensitometer. P.A. Ianna prepared a new version (2005; hereinafter MPRP2) to calculate the parallaxes and proper

motions from observations recorded on CCD's, such as used with the Siding Spring Observatory 1-meter telescope.

The modernized MPRP2 used an iterative three plate-constant adjustment model to calculate the preliminary relative parallaxes and proper motions listed in Table 3.5. To improve the results, the program iterated over the plate constants and relative proper motions seven times for each field. In most cases, small fluctuations in the least significant digit of the resulting relative parallax and proper motions continue with each iteration; the most significant improvements appear in the first few iterations. The mean errors of unit weight range from 0.3 to 0.8 μm, or 7 to 20 milliseconds of arc (mas), with an average of 0.4 ± 0.1 μm, or 10 ± 2 mas, in the x-coordinate (right ascension) and of 0.4 ± 0.1 μm, or 11 ± 3 mas, in the y-coordinate (declination).

Following the removal of proper motion and parallax, the x- and y-residuals associated with each observation were subjected to a time-series analysis using the Lomb-Scargle normalized periodogram method (Press *et al*. 1996). The x- and y-residuals for each single night were combined and a new set of periodograms were calculated for each star. A similar approach was used for the photographic observations of Barnard's Star in Chapter 2. Frequencies up to four times the effective Nyquist frequency were searched; the Nyquist frequency is the highest frequency recoverable from evenly sampled data. Although averaging the data can improve detection efficiency, it also reduces the effective Nyquist frequency, which may drop below the signal frequency and make detection more difficult (Scargle 1982). The effective Nyquist frequency (f_{Neff}) for unevenly sampled data may be expressed as

$$f_{Neff} = \frac{N}{2T} \tag{3.2}$$

where N is the number of observations taken over total time (T). The lowest independent frequency (f_{low}) is

$$f_{low} = \frac{1}{T} \tag{3.3}$$

and the observation time defines a single period. When a companion is suspected, more than a single full orbital period should be observed in order to decouple the linear component of the companion-induced perturbation from the proper motion terms adequately (Black & Scargle 1982). Table 3.8 lists the effective Nyquist and lowest independent frequencies for each star.

3.2.1 Concerns Regarding Time and Parallax Factor Calculations

When graphing the residuals and associated periodograms for LHS 2813 and LHS 3064, a discrepancy in the order of some recent frames was detected. The frame numbers for each field were sequential but the associated observation dates, expressed as fractional years, were not. No other regions had such obvious temporal discontinuities. Acomparison of the handwritten observation logs, the on-line catalogs, and the parallax input files (pif's) indicated that the problem occurred when the observation date was converted to a fractional year during the pif-generation process. The parallax factors, which are calculated based on observation time, were also affected, but the hour angles did not appear to be. The problem appeared to occur during observations that

TABLE 3.8
FREQUENCIES ASSOCIATED WITH AVAILABLE OBSERVATIONS

Star (LHS)	Lowest Independent Frequency (yr^{-1}) All	Lowest Independent Frequency (yr^{-1}) Nightly	Lowest Independent Period (yr) All	Lowest Independent Period (yr) Nightly	Effective Nyquist Frequency (yr^{-1}) All	Effective Nyquist Frequency (yr^{-1}) Nightly	Effective Nyquist Period (yr) All	Effective Nyquist Period (yr) Nightly	Observational Baseline (years)
34	0.14574179	0.1457418	6.8614500	6.861450	7.7243	1.603	0.1295	0.6238	6.8614500
271	0.10023248	0.1002325	9.9768060	9.976806	6.5652	1.353	0.15232	0.7390	9.9768060
288	0.14762488	0.14762754	6.7739260	6.7738040	7.7503	1.329	0.129027	0.7526	6.7739260
337	0.30268991	0.30268991	3.3037110	3.3037110	15.740	2.119	0.063533	0.4720	3.3037110
532	0.14092067	0.31036190	7.0961910	3.2220450	7.0460	2.948	0.14192	0.3392	7.0961910
1134	0.16731000	0.1673134	5.9769290	5.976807	4.266	1.004	0.2344	0.9961	5.9769290
1565	0.15986262	0.1598657	6.2553710	6.255249	6.474	1.439	0.1545	0.6950	6.2553710
2310	0.14942908	0.1494345	6.6921380	6.691894	8.4427	1.494	0.11844	0.6692	6.6921380
2739	0.14016358	0.1401660	7.1345210	7.134399	9.8115	1.682	0.10192	0.5945	7.1345210
2813	0.12253201	0.1225320	8.1611330	8.161133	8.3322	1.164	0.12002	0.8591	8.1611330
3064	0.12257051	0.1225742	8.1585690	8.158325	7.4155	0.981	0.13485	1.02	8.1585690
3242	0.14173746	0.1417424	7.0552980	7.055054	9.0003	1.417	0.11111	0.7055	7.0552980
3418	0.15624644	0.1562494	6.4001460	6.400024	9.6092	1.562	0.10407	0.6400	6.4001460

spanned local midnight. In addition to the obvious discontinuities initially discovered within the files for the two specific regions, the discontinuity in one field was found to continue in the observations of another field. In this case, the observations of LHS 2813 suffered a discontinuity at local midnight. Observations of LHS 3064 immediately followed LHS 2813 and continued the incorrect times. Identifying this more subtle type of temporal reversal in the other regions would require checking each observation.

As of 2006 June 29, the data reduction software was still being investigated for the source of these errors and an eventual program-wide solution (M. Begam 2006, private communication). To circumvent this problem, a stand-alone program, "pfonly," was used to calculate the fractional year and parallax factors manually for each frame of LHS 2813 and LHS 3064. The existing times and parallax factors were compared with the new values and the pif's updated appropriately. Eventually, 4 out of 136 frames for LHS 2813 and 39 out of 121 frames for LHS 3064 were changed; the average magnitude of the changes was 0.0021 ± 0.0012 year and 0.0024 ± 0.0052 in parallax factor. Although LHS 288 lacks an obvious discontinuity, its observation times and parallax factors were checked against pfonly-calculated values because its periodograms are noisy. As a result of this check, no frames for LHS 288 were changed.

New relative parallaxes and proper motions for LHS 2813 and LHS 3064 were calculated based on the revised times and parallax factors. Table 3.9 compares the relative parallaxes and proper motions obtained from the uncorrected data to those obtained after the corrections. The changes are all within the errors of the original values.

TABLE 3.9

EFFECT OF CORRECTIONS FOR TEMPORAL DISCONTINUITY IN DATA

Star (LHS)	Parallax (mas) Uncorrected	Parallax (mas) Corrected	Proper Motion (mas yr^{-1}) Uncorrected	Proper Motion (mas yr^{-1}) Corrected	Position Angle (deg) Uncorrected	Position Angle (deg) Corrected	Comment
2813	59.9 ± 1.7	59.8 ± 1.7	533.80 ± 0.60	533.72 ± 0.60	138.615 ± 0.064	138.608 ± 0.064	changes in y-coordinate
3064	82.7 ± 1.0	82.7 ± 1.0	729.16 ± 0.47	729.00 ± 0.47	36.108 ± 0.034	36.117 ± 0.034	changes in y-coordinate

The residuals from updated relative parallax and proper motion were, then, subjected to time-series analysis as discussed earlier.

Before the publication of the final SPP parallaxes and proper motions (BIP), the year fraction and parallax factors for each observation will need to be verified. The time-series analysis used herein to identify possible perturbations is not as sensitive to small errors in these values. The order of the residuals is more important than the time of observation with which they are associated. Beutler (1970) demonstrated that a power spectrum may be estimated when only the sampling order is recorded for an infinite baseline. Correcting LHS 2813 and LHS 3064 restored temporal order to the plate sequences; the discontinuities might otherwise have seriously affected the detection of a perturbation. None of the other fields appear to have frames out of order; LHS 288 was manually checked and found to be free of this particular error. Therefore, no other fields were manually corrected.

3.2.2 Periodograms

None of the periodograms calculated for any of the stars clearly indicated the presence of any unseen companions. LHS 288 and 2813 showed some interesting features in the preliminary analysis (Bartlett, Ianna, & Begam 2002), and LHS 288 retains most of them at the end of this final reduction.

Significant peaks in both the x- and y-residual periodograms at the same frequency would indicate the possible presence of a companion. In rare cases, such as an orbital inclination near 90 degrees (°), a strong peak in only one coordinate might also signal the presence of a companion. When the individual residuals are combined

into nightly normal points, the resulting periodograms should also show similar peaks. Parallax observations are made primarily in the morning and evenings and in this case were usually scheduled during bright observing time. The cyclical nature of this observing schedule may produce signals at frequencies close to the synodic month, six months, and one year (Black & Scargle 1982).

When individual observations are considered, a larger range of frequencies is sampled than when nightly normal points are analyzed. Therefore, some high-frequency peaks in the periodograms for individual residuals cannot be compared with similar points on the periodograms for nightly residuals. In all cases, the high frequencies correspond to periods less than one year, which are most likely spurious. Because in most cases the effective Nyquist frequency corresponds to periods of less than one year, the algorithm may extract potential periods less than a year. However, astrometric techniques are more sensitive to long-period planets (Quirrenbach *et al*. 2004).

3.2.2.1 LHS 34

Although the other stars in this study are M dwarfs, LHS 34 is a white dwarf. Its reasonable parallax and moderate coverage were sufficient to include it in the second subsample; Figure 3.2 illustrates the residuals for LHS 34. It also has the highest measured proper motion of any star in this study. DCR corrections were not applied to LHS 34 as explained in Table 3.7. However, it was observed in I-band, where atmospheric refraction is minimal (Jao *et al*. 2005)

A white dwarf may not appear as an ideal primary to host planetary companions, but they do appear in binaries and are, therefore, worth investigating. Farihi, Becklin,

and Zuckerman (2005) identified two L-dwarf companions and nine M-dwarf companions later than spectral type M4.5 in a survey of 261 white dwarfs. In addition, a planet with a projected mass (mass times the sine of an unknown inclination angle, m sin *i*) 2.5 times greater than that of Jupiter (M_{2l}) orbits the neutron star-white dwarf binary system, PSR B1620-26 + WD J1623-266 (Thorsett, Arzoumanian, & Taylor 1993; Joshi & Rasio 1997) while a neutron star, PSR 1257+12, appears to host a system of several planets (Wolszczan & Frail 1992). However, LHS 34 does not appear to have companions, as shown in Figure 3.3.

At best, the periodograms for LHS 34 hint at something occurring with a period of 2–2.5 years; the minimum detectable companion by this study would have a mass of 13.8 ± 0.8 M_{2l} as discussed in section 3.2.2. No spectral peak is clearly of physical origin and most probably arise from noise alone; Table 3.10 lists the major features of the periodograms for individual and nightly residuals in x and y. The all x- and y-periodograms have points at a frequency of 0.47366 yr^{-1}, which corresponds to a period of 2.1112 years, with a greater than 50% chance of being real but the corresponding points in the periodograms for nightly residuals do not. The maximum power in the nightly x-residuals is found nearby at a frequency of 0.4008 yr^{-1}, which corresponds to a period of 2.495 years, and has a greater than 50% chance of being real. Although the corresponding point of the all x-residual periodogram is a local peak, the corresponding points in both y-periodograms have a less than 50% chance of being real.

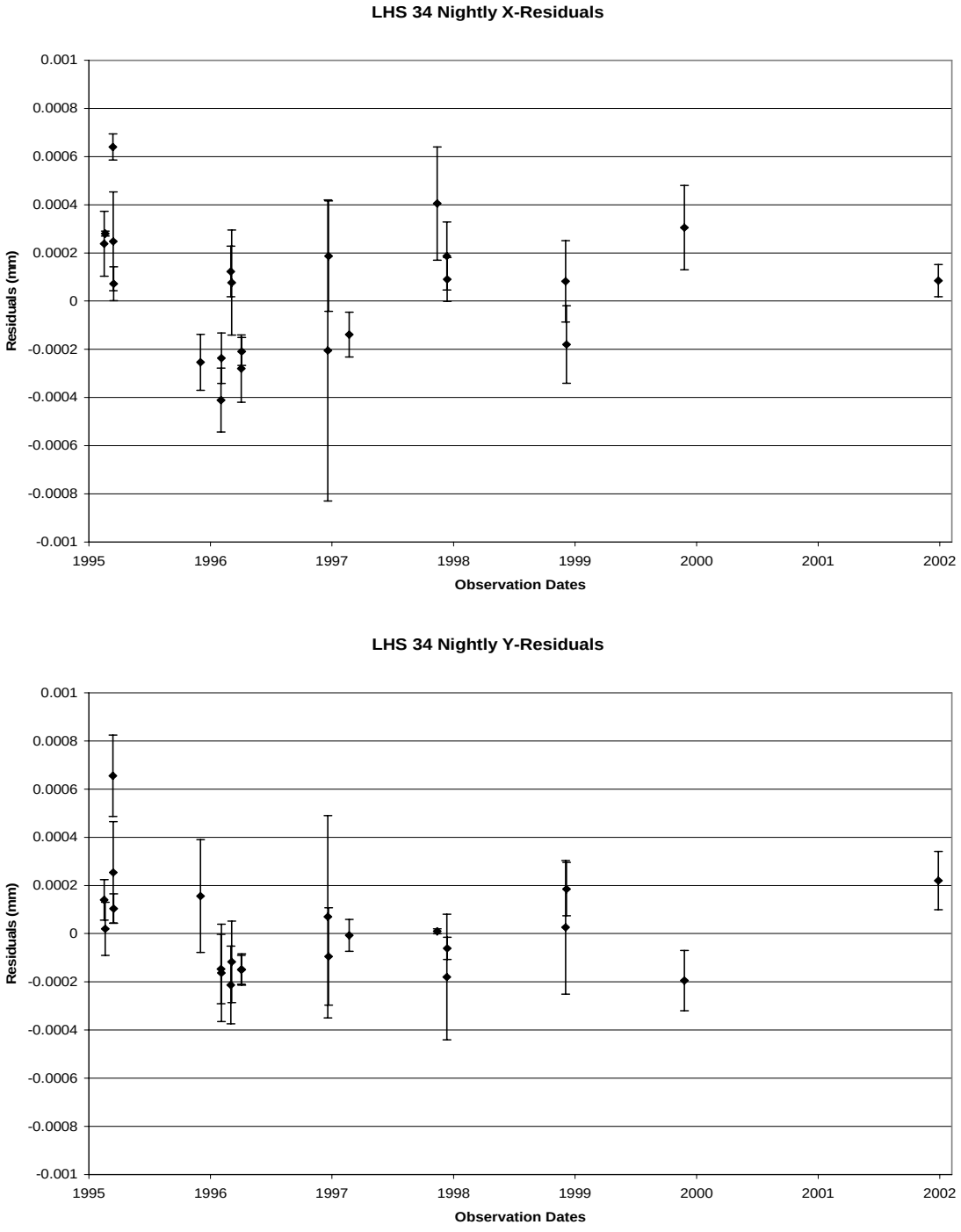

FIG. 3.2.—Nightly X- and Y-Residuals for LHS 34. Top chart contains x-residuals averaged by night. Bottom chart contains y-residuals averaged by night.

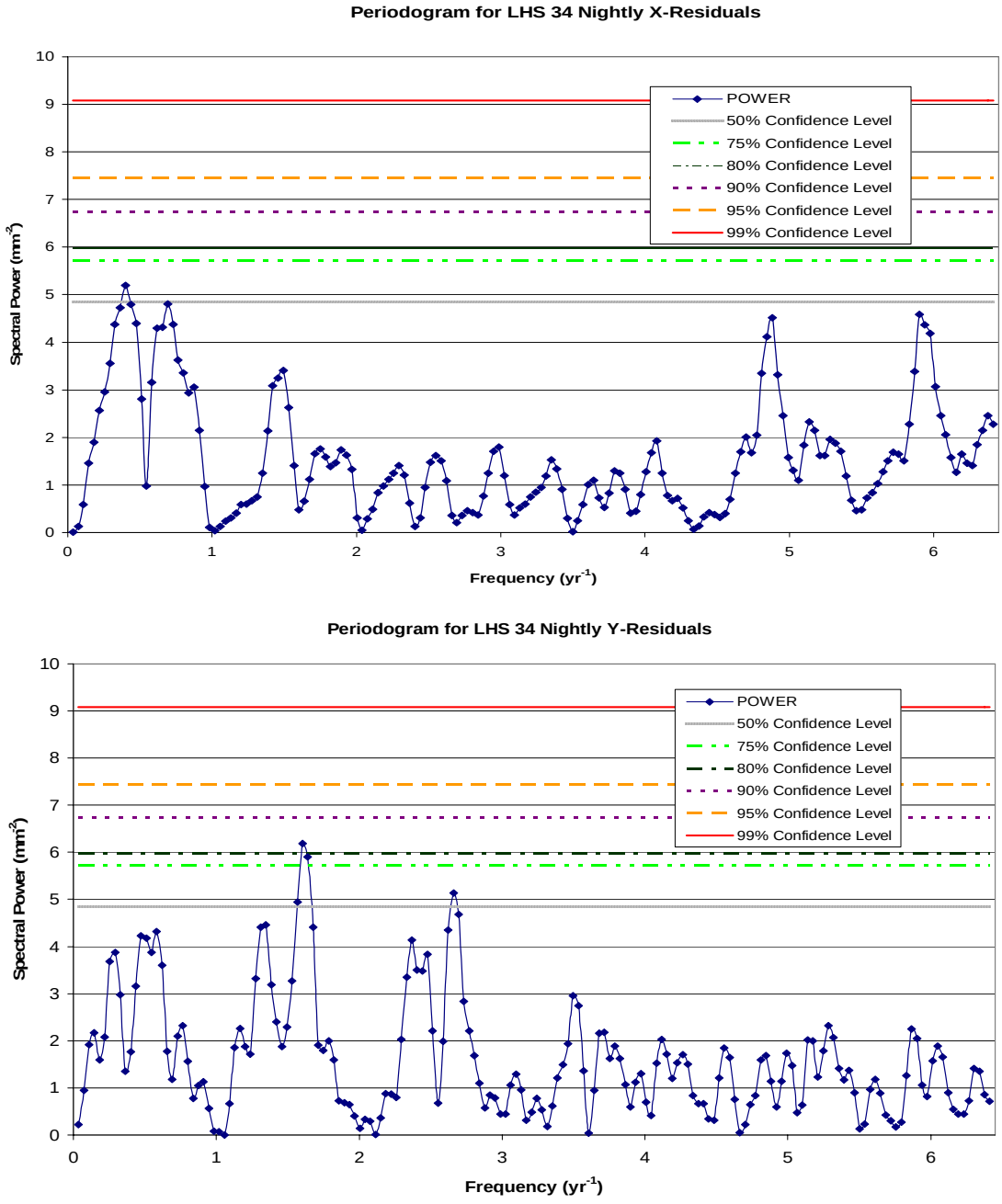

Fig. 3.3.— LHS 34 Periodograms. Top chart is a periodogram calculated for nightly x-residuals. Bottom chart is a periodogram calculated for nightly y-residuals. Horizontal lines in the periodograms indicate likelihood that spectral peaks exceeding that power are real and not caused by noise only. Solid line is 99% confidence, dashed line 95% confidence, dotted line 90% confidence, dash dotted line is 80% confidence, dash double-dotted line is 75% confidence, and hashed line is 50% confidence.

TABLE 3.10
FEATURES OF PERIODOGRAMS FOR LHS 34

Feature	Frequency (yr^{-1})	Period (yr)	Power (mm^{-2})	False Alarm Probability (%)	Comment
All X, maximum	28.748	0.034786	11.115	<1	frequency too high for nightly x
All X, local peak	0.40079	2.4951	9.0149	<10	corresponds to maximum in nightly x
All X	0.47366	2.1112	7.8254	<20	corresponds to local peak in all y
All Y, maximum	1.6032	0.62377	8.4863	8	matches maximum in nightly y
All Y	0.40079	2.4951	3.3113	<50	corresponds to maximum in nightly y
All Y, local peak	0.47366	2.1112	6.4906	<50	
Nightly X, maximum	0.4008	2.495	5.199	39	corresponds to local peak in all x
Nightly X	0.4737	2.111	4.397	>50	corresponds to local peak in all y
Nightly Y, maximum	1.603	0.6238	6.181	17	matches maximum in all y
Nightly Y	0.4737	2.111	4.227	>50	corresponds to local peak in all y

3.2.2.2 LHS 271

LHS 271, a M4.5 V star (Henry *et al*. 2002), has the longest baseline and was observed on the most nights of any of the stars in this study. This coverage along with an adequate parallax solution prompted the inclusion of LHS 271 in the second sample. Jao *et al*. (2005) determined an absolute parallax of 153 ± 2 mas and a relative proper motion of 1.120 ± 0.003" yr^{-1} in 365.7 ± 0.2°, which generally agrees with the preliminary relative parallax and proper motion listed in Table 3.5

Figure 3.4 illustrates the residuals that were calculated without the benefit of DCR corrections as discussed in Table 3.7. DCR is a concern for LHS 271, which was observed through the R_C filter and for which 18% of the exposures used were taken at large hour angles. DCR is greatest for red stars observed in R-band (Jao *et al*. 2005). The SPP also made eighty-two I-band observations of LHS 271 but the error associated with the resulting parallax was greater than 3 mas (156.9 ± 4.4 mas) and the baseline was much shorter (4.8 years).

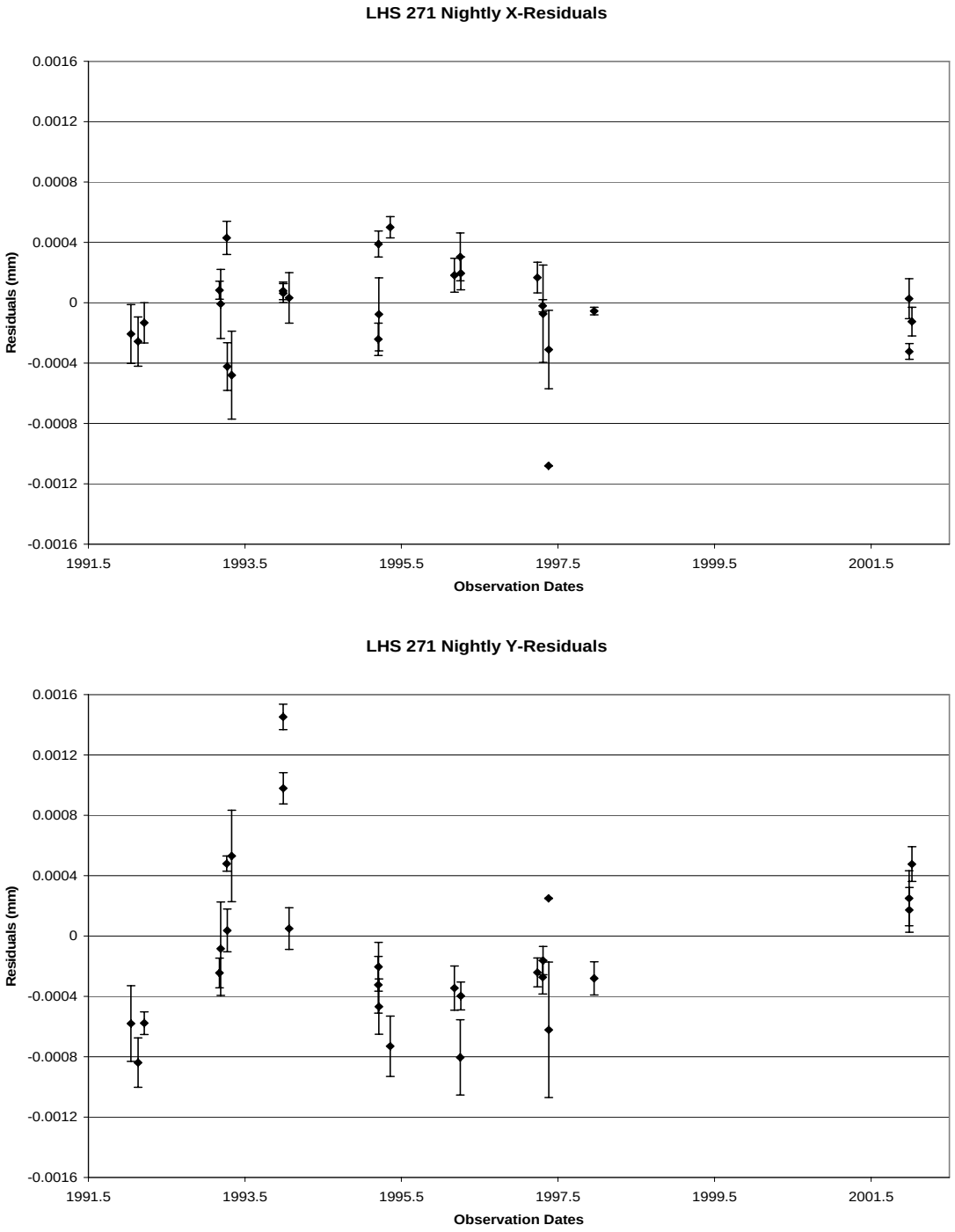

FIG. 3.4.— Nightly X- and Y-Residuals for LHS 271. Top chart contains x-residuals averaged by night. Bottom chart contains y-residuals averaged by night.

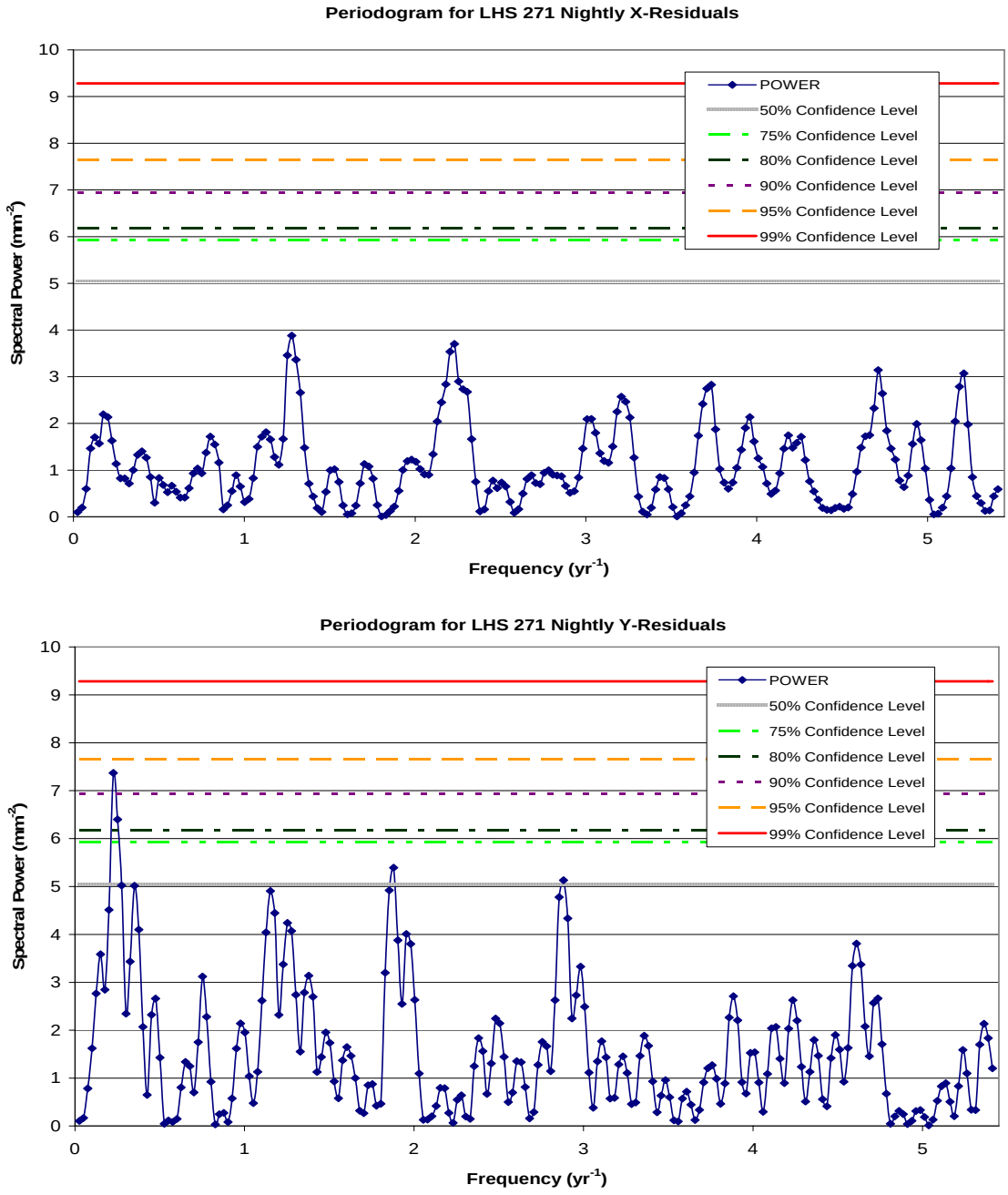

FIG. 3.5.— LHS 271 Periodograms. Top chart is a periodogram calculated for nightly x-residuals. Bottom chart is a periodogram calculated for nightly y-residuals. Horizontal lines in the periodograms indicate likelihood that spectral peaks exceeding that power are real and not caused by noise only. Solid line is 99% confidence, dashed line 95% confidence, dotted line 90% confidence, dash dotted line is 80% confidence, dash double-dotted line is 75% confidence, and hashed line is 50% confidence.

TABLE 3.11
FEATURES OF PERIODOGRAMS FOR LHS 271

Feature	Frequency (yr^{-1})	Period (yr)	Power (mm^{-2})	False Alarm Probability (%)	Comment
All X, maximum	23.655	0.042275	7.6379	22	frequency too high for nightly x
All X, local peak	0.20047	4.9884	5.3863	>50	adjacent to frequency of interest
All X, adjacent to local peak	0.22552	4.4341	3.7702	>50	corresponds to maxima in y
All X, local peak	1.2780	0.78249	5.0507	>50	corresponds to maximum in nightly x
All Y, maximum	0.22552	4.4341	32.103	<1	matches maximum in nightly y
All Y, local peak	1.2780	0.78249	14.138	<1	corresponds to maximum in nightly x
Nightly X, maximum	1.278	0.7825	3.879	90	corresponds to weak local peak in all x
Nightly X	0.2255	4.434	1.629	>50	corresponds to maxima in y
Nightly Y, maximum	0.2255	4.434	7.370	7	matches maximum in all y
Nightly Y, local peak	1.253	0.7981	4.238	>50	adjacent to frequency of interest
Nightly Y, adjacent to local peak	1.278	0.7825	4.071	>50	corresponds to maximum in nightly x

LHS 271 does not appear to have any unseen companions as shown in Figure 3.5. As discussed in section 3.2.3, the minimum detectable companion by this study would have a mass of 4.8 ± 0.8 M_{2l}. Table 3.11 lists the important features of the periodograms. Although the maximum peaks in both y-periodograms occur at a frequency of 0.2255 yr^{-1}, which corresponds to a 4.434-yr period, no significant power appears at that frequency on either of the x-periodograms. Some orbital orientations to our line of sight might result in a perturbation of only one coordinate; however, such alignments are unlikely.

3.2.2.3 LHS 288

LHS 288 was an intriguing candidate in the preliminary analysis (Bartlett, Ianna, & Begam 2002) that continues to perplex. It is a nearby, M5.5 V star (Bessell 1991). The photographic SPP previously measured an absolute parallax of 221 ± 8 mas, which puts it at a distance of about 4.5 pc, and a relative proper motion of 1.648 ± 0.005 seconds of arc (") yr^{-1} in 347.6 ± 0.1° with the Yale-Columbia 66-centimeter refractor at Mount Stromlo Observatory (Ianna & Bessell 1986). Recent results from the Cerro Tololo Inter-American Observatory Parallax Investigation (CTIOPI) place it slightly farther away with an absolute parallax of 209 ± 3 mas but similar proper motion of 1.643 ± 0.001" yr^{-1} in 347.70 ± 0.07° (Henry *et al*. 2006)

As part of the CCD program, LHS 288 was imaged 105 times on 18 nights between 1991 May and 1998 March using the R_C filter; however, only 104 images were used for the preliminary periodograms. Figure 3.1 shows the results of the preliminary analysis along with some estimates of the potential perturbations due to hypothetical

brown dwarf companions. The periodograms calculated for LHS 288 were dramatically noisier than any of the others. Significant power appeared to be present at frequencies of 0.14751 and 0.29501 yr^{-1}, which correspond to periods of 6.7794 and 3.3897 years, in the all x- and all y-periodograms. Because the longer period is twice the shorter, these peaks may be related. The nightly x- and y-periodograms have features on either side of 0.2950 yr^{-1}, a local peak in the nightly x-periodogram and the maximum peak in the nightly y-periodogram. While the features in the periodograms for all residuals have a greater than 99% chance of being real, the corresponding features in the periodograms for nightly normal points have a less than 50% chance. Although the features are most likely spurious, the initial results bore further investigation in order to understand all the features presented.

LHS 288 was one of the first fields reduced using CCD images during the SPP. Therefore, some changes in software and methodologies occurred during its reduction, (M. Begam 2002, private communication; P. Ianna 2002, private communication). To eliminate these changes in the data reduction pipeline as a possible noise source in LHS 288 periodograms, LHS 288 was re-reduced beginning with the archived, flat-fielded images.

During this re-analysis of the LHS 288 field, all 105 images were used. DCR corrections were applied to LHS 288 and its eleven reference stars, which are identified in Figure 3.6 and Table 3.12. Ianna and Bessell (1986) used a magnitude term in addition to the standard three-plate constant model to improve the earlier

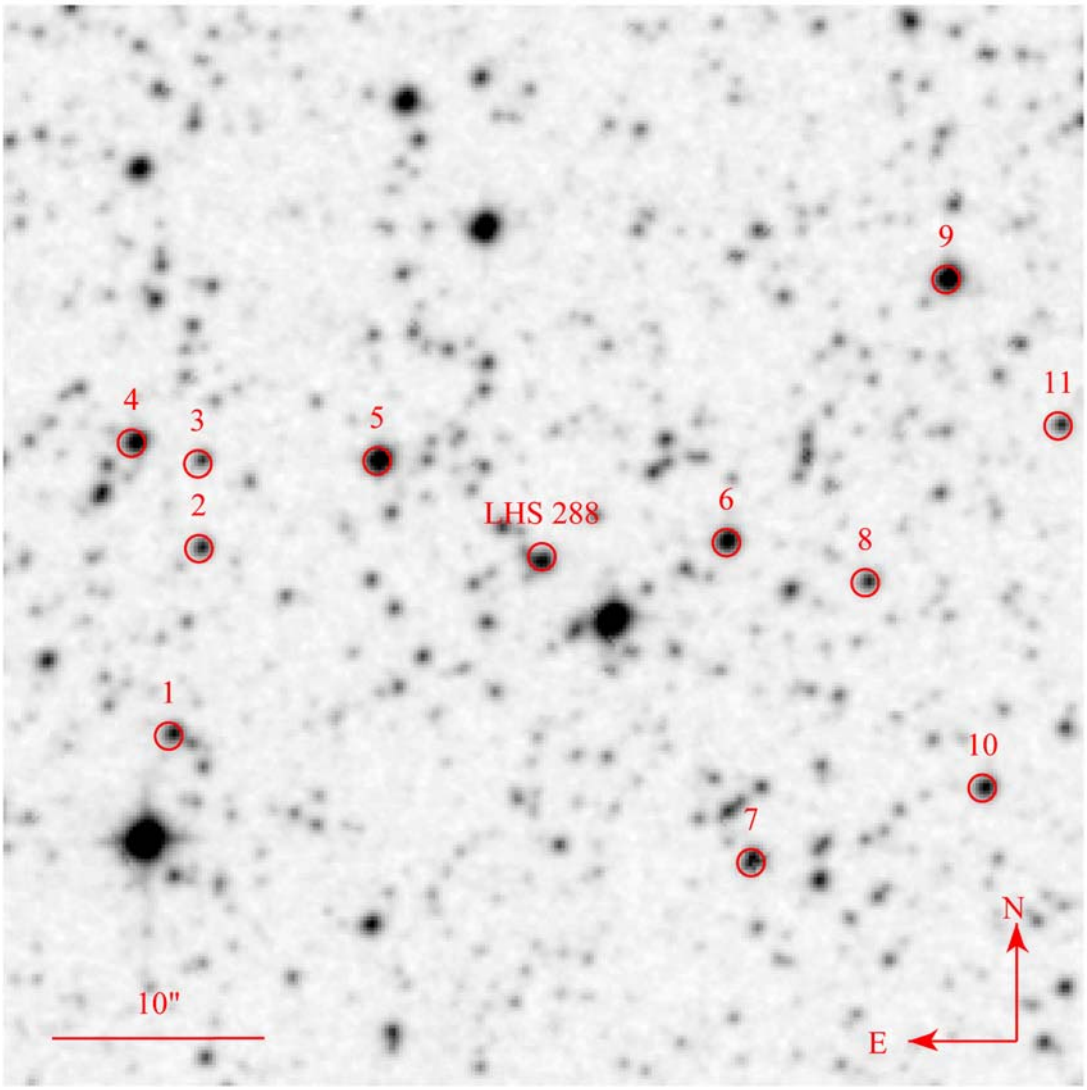

FIG. 3.6.— LHS 288 and Reference Frame. Image Source: Second Generation Digitized Sky Survey via *SkyView* with annotations by J. L. Bartlett & J. L. Bartlett. Image © 1993-2004 Anglo-Australian Observatory Board; compressed and distributed by the Space Telescope Science Institute.

parallax measurement of LHS 288. When MPRP2 calculated the relative parallax and proper motion of LHS 288, additional terms were considered for inclusion in the plate adjustment model

$$\begin{aligned} \varepsilon &= ax + by + c + gm + hmx + kC \\ \eta &= dx + ey + f + lm + nmy + pC \end{aligned} \tag{3.4}$$

where (x, y) are the coordinates of the reference star in the system of its own plate; (ε,η) are the coordinates of the reference stars in the system of the trail plate; a, b, c, d, e, f, g, h, k, l, n, p are the plate constants; m is the apparent magnitude of the reference star; and, C is the color of the reference star. The potential terms of magnitude (gm, lm), coma (hmx, nmy), and color (kC, pC) were tested individually based on the photometry listed in Table 3.12; Patterson, Ianna, and Begam (1998) describe the reduction of SPP photometry to the Cousins system (Bessell 1995; Bessell 1990; Menzies *et al*. 1989; Cousins 1980a; Cousins 1980b; hereafter Cousins). The photometry for LHS 288 is consistent with other published values listed in Table 3.13. Table 3.14 summarizes the results; the number of frames for which a particular higher order term was considered statistically significant out of the 105 total frames is listed for each term separately by coordinate. A prospective term was considered statistically significant for a particular frame if the calculated coefficient was greater than three times the associated error; the probability of such a comparatively large coefficient arising from noise alone is less than 1% (Beers 1957). Although coma is generally reduced in a Ritchey-Chrétien

TABLE 3.12
PHOTOMETRY OF REFERENCE STARS FOR LHS 288

Star	2MASS Designation[a]	V_C (mag)[b]	R_C (mag)[b]	I_C (mag)[b]	$(R-I)_C$ (mag)[b]
Reference 1	10443567-6113281	13.648 ± 0.008	13.044 ± 0.007	12.56 ± 0.008	0.48
Reference 2	10443450-6112361	13.900 ± 0.007	13.529 ± 0.009	13.20 ± 0.020	0.33
Reference 3	10443454-6112125	14.180 ± 0.010	13.960 ± 0.020	13.95 ± 0.040	0.01
Reference 4	10443709-6112067	12.297 ± 0.001	12.182 ± 0.002	12.03 ± 0.005	0.15
Reference 5[c]	10442763-6112120	…	11.437 ± 0.001	11.13 ± 0.003	0.31
Reference 6	10441423-6112345	13.037 ± 0.003	12.305 ± 0.003	11.57 ± 0.004	0.73
Reference 7	10441326-6114033	13.819 ± 0.007	12.998 ± 0.004	12.21 ± 0.006	0.79
Reference 8	10440888-6112456	15.050 ± 0.010	13.396 ± 0.007	11.62 ± 0.004	1.78
Reference 9[d]	10440577-6111215	…	11.386 ± 0.001	11.19 ± 0.003	0.20
Reference 10	10440438-6113425	13.244 ± 0.003	12.932 ± 0.006	12.60 ± 0.008	0.33
Reference 11	10440148-6112019	14.800 ± 0.010	13.890 ± 0.010	12.92 ± 0.010	0.97
LHS 288	10442131-6112384	13.966 ± 0.007	12.306 ± 0.003	10.33 ± 0.001	1.98

NOTES.—[a]2MASS designations have the form hhmmss.ss-ddmmss.s

[b]The errors listed herein are from the raw fitting based on the standard stars observed. Based on other SPP photometry, the expected internal error for $V_C \sim \pm 0.02$ mag, external error for $V_C \sim \pm 0.04$ mag, and the error of the fit $\sim \pm 0.02$ mag.

[c]Reference star 5 is also Tycho 8957-3132-1.

[d]Reference star 9 is also Tycho 8957-1309-1.

REFERENCE.—Photometry is from BIP with SPP errors from Patterson, Ianna, & Begam (1998). Other designations are from 2MASS and Høg *et al*. 2000.

reflector and by the small field, the R and I coma terms appeared significant in x (right ascension). Early frames were taken with no guiding until the autoguider system on the 1-meter telescope was functioning properly and reliably (P. Ianna 2006, private communication). Insufficient guiding could produce positional errors that are a function of magnitude (Schlesinger 1910). No extra term produced a significant improvement in the overall parallax and proper motion solution; consequently, none were used in the final reduction.

TABLE 3.13
COMPARISON OF LHS 288 PHOTOMETRY

Source	V_C (mag)	R_C (mag)	I_C (mag)	$(R-I)_C$ (mag)	Ref
SPP[a]	13.966 ± 0.049	12.306 ± 0.049	10.330 ± 0.057	1.98	1
RECONS	13.90[b] ± 0.03	12.31 ± 0.03	10.27 ± 0.03	2.04	2
Bessell	13.92 …	12.33 …	10.31 …	2.02	3

NOTES.—[a]Errors for SPP values are estimated from 4.
[b]V_{JM} is quoted here. It is substantially the same as V_C according to 5.
REFERENCES.—(1) BIP; (2) Henry *et al*. 2004; (3) Bessell 1991; (4) Patterson, Ianna, & Begam 1998; (5) Bessell & Weis 1987

TABLE 3.14
ADDITIONAL PLATE MODEL TERMS CONSIDERED FOR LHS 288

Term	Significant in X? (frames)	(percent)	Significant in Y? (frames)	(percent)	Comment
V magnitude	…		…		not tested, incomplete photometry
R magnitude	69	66	13	12	improved solution insignificantly
I magnitude	49	47	8	8	term statistically insignificant
R coma	71	68	13	12	improved solution insignificantly
I coma	68	65	12	11	solution slightly worsened
R-I color	3	3	0	0	term statistically insignificant

NOTE.—A total of 105 frames were used for LHS 288.

Although the LHS 288 pif did not contain any obvious temporal discontinuities like those found for LHS 2813 and LHS 3064, the observation year fraction and

parallax factors were manually checked for each observation as discussed in 3.2.1. No problems were found with any of these values.

The values listed in Table 3.5 were determined after seven iterations when the solutions appeared to converge; five individual residuals greater than 1 μm resulted but all nightly residuals were less than 1 μm. Skipping the frame with the largest residual produced a slightly better solution overall but the image itself, the observing log, and the reduction notes provide no reason for doing so and it was retained. In half the images taken that particular night, reference star 9 was definitely saturated and dropped from the reduction. On further examination of the images, the contours of reference star 5 and 9 indicated possible saturation. However, dropping reference stars 5 and 9 from those frames worsened the solution so these stars were retained.

The residuals from the final reduction of LHS 288 are shown in Figure 3.7, individually, and in Figure 3.8, combined into nightly normal points. Figure 3.9 and Figure 3.10 are the corresponding periodograms. The highest power in both x-periodograms occurs at 0.2952 yr^{-1}, which corresponds to a 3.4-year period, with a greater than 80% chance of being real in both cases. The corresponding frequency in the periodogram for all y-residuals has a greater than 99% chance of being real and is adjacent to a local peak. The highest power in both y-periodograms occurs at 0.1476 yr^{-1}, which corresponds to a 6.8-year period, with a greater than 80% chance of being real in both cases. The corresponding frequency in the periodogram for all x-residuals has a greater than 99% chance of being real and is adjacent to a local peak. Aliasing

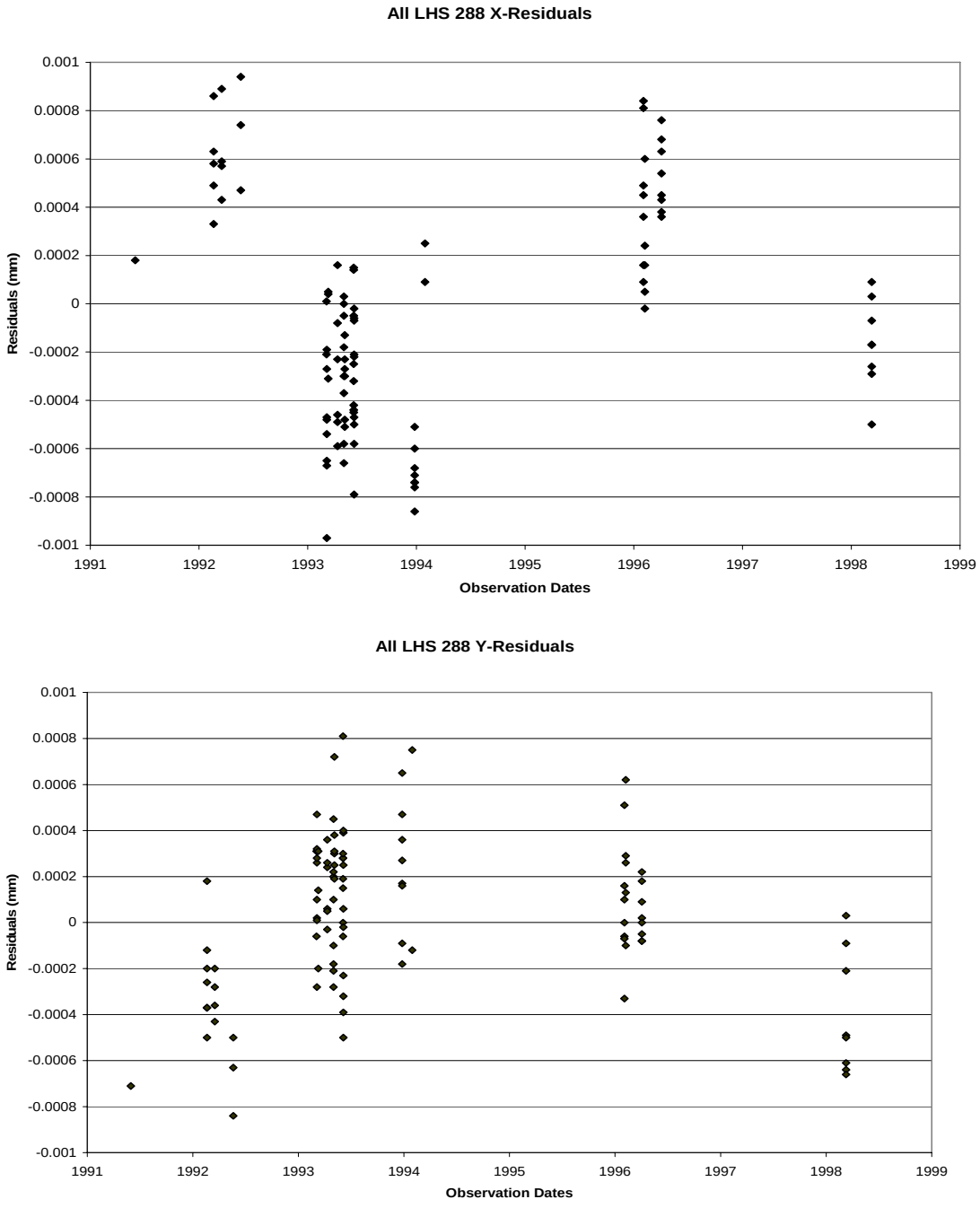

FIG. 3.7.— All X- and Y-Residuals for LHS 288. Top chart contains all x-residuals. Bottom chart contains all y-residuals.

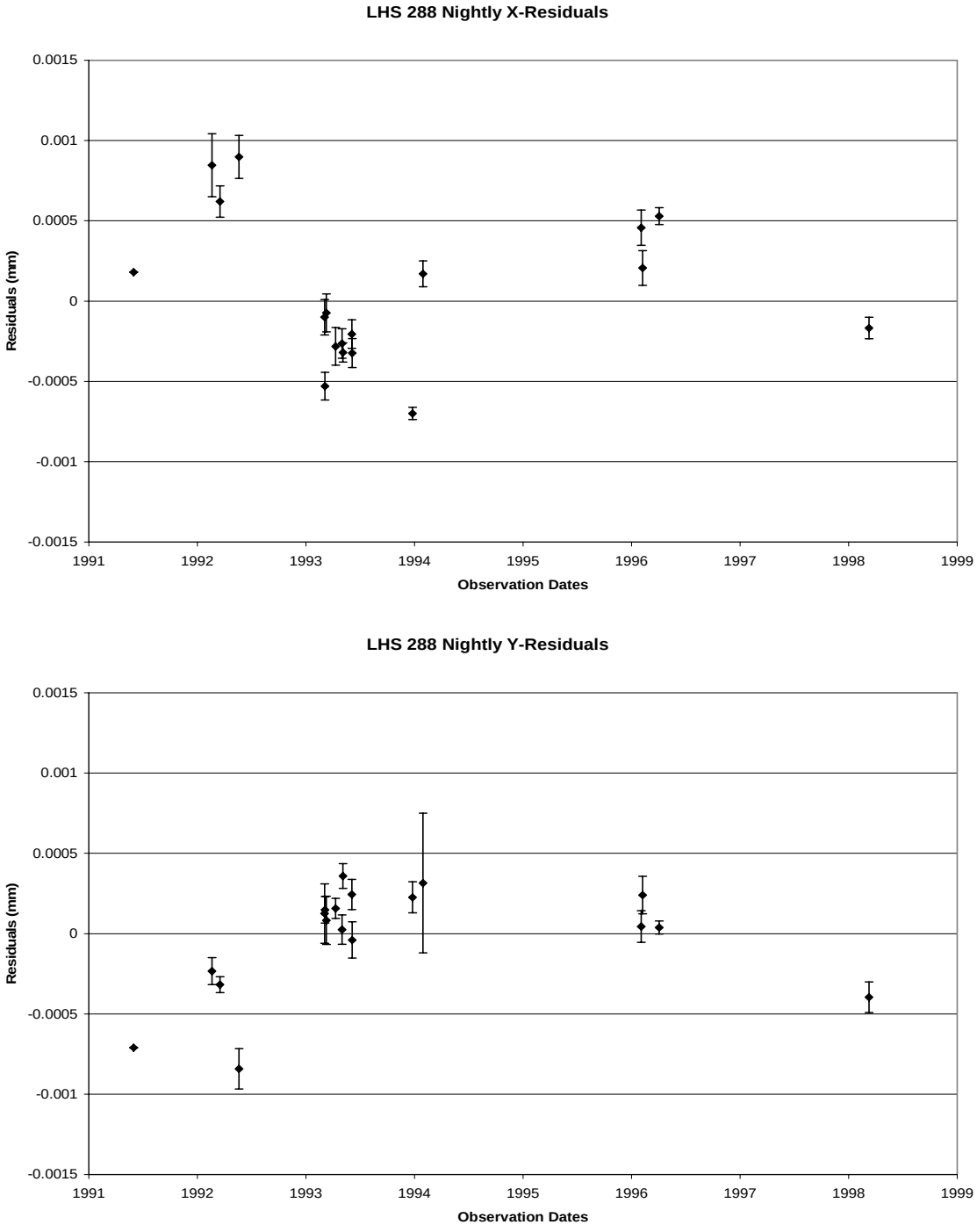

FIG. 3.8.—Nightly X- and Y-Residuals for LHS 288. Top chart contains x-residuals averaged by night. Bottom chart contains y-residuals averaged by night.

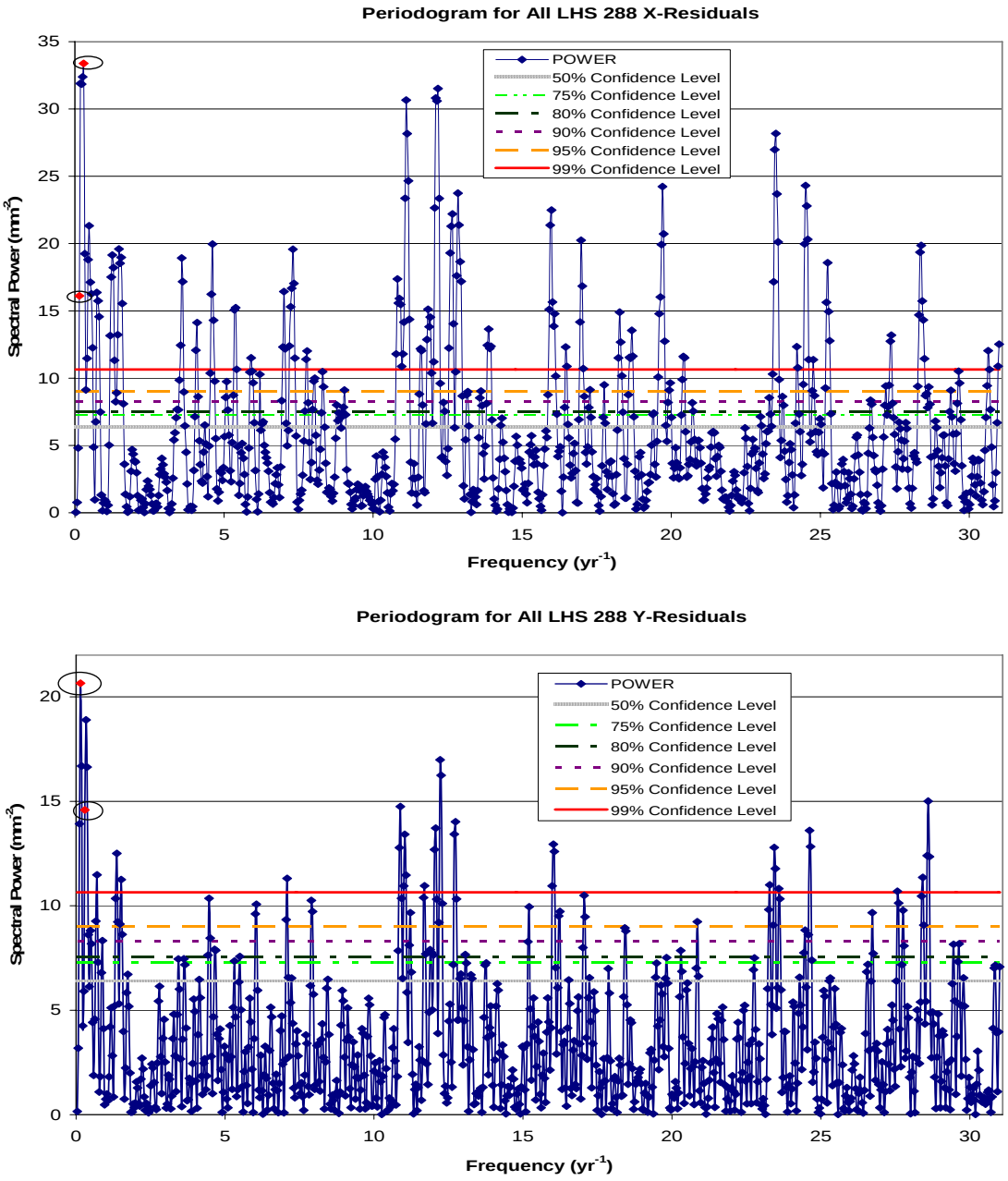

FIG. 3.9.—LHS 288 Periodograms. Top chart is a periodogram calculated for all x-residuals. Bottom chart is a periodogram calculated for all y-residuals. Ovals mark points of interest implying a companion with an orbit of 3.4 or 6.8 years. Horizontal lines in the periodograms indicate likelihood that spectral peaks exceeding that power are real and not caused by noise only. Solid line is 99% confidence, dashed line 95% confidence, dotted line 90% confidence, dash dotted line is 80% confidence, dash double-dotted line is 75% confidence, and hashed line is 50% confidence.

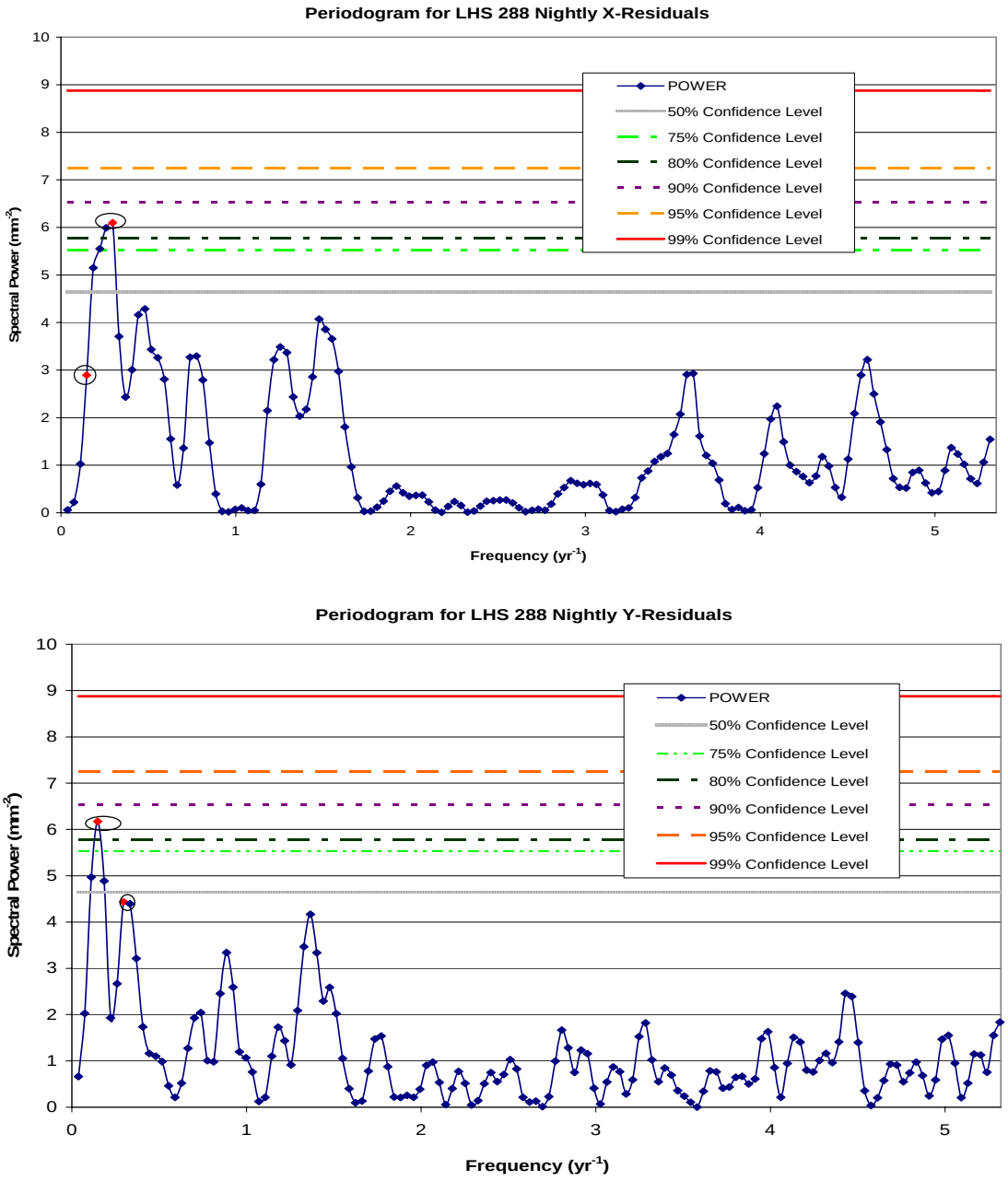

FIG. 3.10.—LHS 288 Nightly Periodograms. Top chart is a periodogram calculated for nightly x-residuals. Bottom chart is a periodogram calculated for nightly y-residuals. Ovals mark points of interest implying a companion with an orbit of 3.4 or 6.8 years. Horizontal lines in the periodograms indicate likelihood that spectral peaks exceeding that power are real and not caused by noise only. Solid line is 99% confidence, dashed line 95% confidence, dotted line 90% confidence, dash dotted line is 80% confidence, dash double-dotted line is 75% confidence, and hashed line is 50% confidence.

TABLE 3.15
FEATURES OF PERIODOGRAMS FOR LHS 288

Feature	Frequency (yr^{-1})	Period (yr)	Power (mm^{-2})	False Alarm Probability (%)	Comment
All X, maximum	0.29525	3.3870	33.380	<1	matches maximum in nightly x
All X, adjacent to local peak	0.14762	6.7739	16.116	<1	corresponds to maxima in y
All X, local peak	0.18453	5.4192	31.895	<1	adjacent to frequency of interest
All Y, maximum	0.14762	6.7739	20.651	<1	matches maximum in nightly y
All Y, adjacent to local peak	0.29525	3.3870	14.581	<1	corresponds to maxima in x
All Y, local peak	0.33216	3.0106	18.898	<1	adjacent to frequency of interest
Nightly X, maximum	0.2953	3.387	6.099	15	matches maximum in all x
Nightly X	0.1476	6.774	2.895	>50	corresponds to maxima in y
Nightly Y, maximum	0.1476	6.774	6.173	14	matches maximum in all y
Nightly Y, local peak	0.2953	3.387	4.435	>50	corresponds to maxima in x

can move spectral power to a lower frequency than the actual signal but is generally reduced by uneven sampling (Scargle 1982) like the observations of LHS 288. Table 3.15 lists the features of the periodograms for LHS 288.

The periodograms for LHS 288 may indicate a perturbation with a 3.4-year or 6.8-year period. These potential signals are stronger than any others detected in this study. However, they do not clearly indicate the presence of an unseen companion. The multiplication of the residuals by an appropriate data windowing function might reduce any spectral leakage present and smooth the periodogram further (Scargle 1982). With its low mass and proximity to the Earth, a Jupiter-mass planet orbiting LHS 288 with these periods would produce perturbations of 2–3 mas as discussed in 3.2.3.2. The minimum detectable planet in this study would be $2.4 \pm 0.7\ M_{2\downarrow}$. Because LHS 288 is a high proper-motion star in a rich field, the possibility that it passed over an undetected faint star during the SPP observations cannot be eliminated; such a distorted point-spread function might mimic a perturbation. Additional observations from an independent data set would provide the best determination of the validity of these spectral peaks. The Research Consortium on Nearby Stars (RECONS 2006, private communication) remains interested in LHS 288 as a potential planetary host and continues to observe it at CTIO. Observing it with the Fine Guidance Sensors (FGS) of the Hubble Space Telescope (HST) would be another possibility.

3.2.2.4 LHS 337

LHS 337 is a nearby, M4.5 V (Hawley, Gizis, & Reid 1996), high-proper motion star at a distance of about 6.9 pc (BIP). Recent CTIOPI results place it slightly closer with an absolute parallax of 157 ± 2 mas and proper motion of 1.464 ± 0.002" yr^{1} in 206.4 ± 0.1º (Henry *et al*. 2006). As shown in Figure 3.1, LHS 337, along with LHS 1565, served as an example of a star with no hint of perturbation detected by the preliminary analysis. It has the shortest baseline of any star in this study, only 3.3 years. However, it was imaged 104 times on 14 nights resulting in a relative parallax with an error less than 1.5 mas and mean errors of unit weight less than 0.5 μm; these error values fall in the mid-range of such errors in this study. Earlier SPP photometry can be found in Table 3.6.

Before calculating the final periodograms, DCR corrections were applied to LHS 337 and its reference stars. As shown in Figure 3.11 and Figure 3.12, LHS 337 still shows no sign of any perturbation. Any companion would need to be less than 6 ± 1 M_{Jup} as discussed in 3.2.3. Table 3.16 lists the features of the periodograms for LHS 337, all of which correspond to periods of less than one year and are most likely the result of noise. No point in the periodograms for nightly residuals has a 50% or greater possibility of being real. Jao *et al*. (2003) found no companions to LHS 337 during an examination of CTIOPI images.

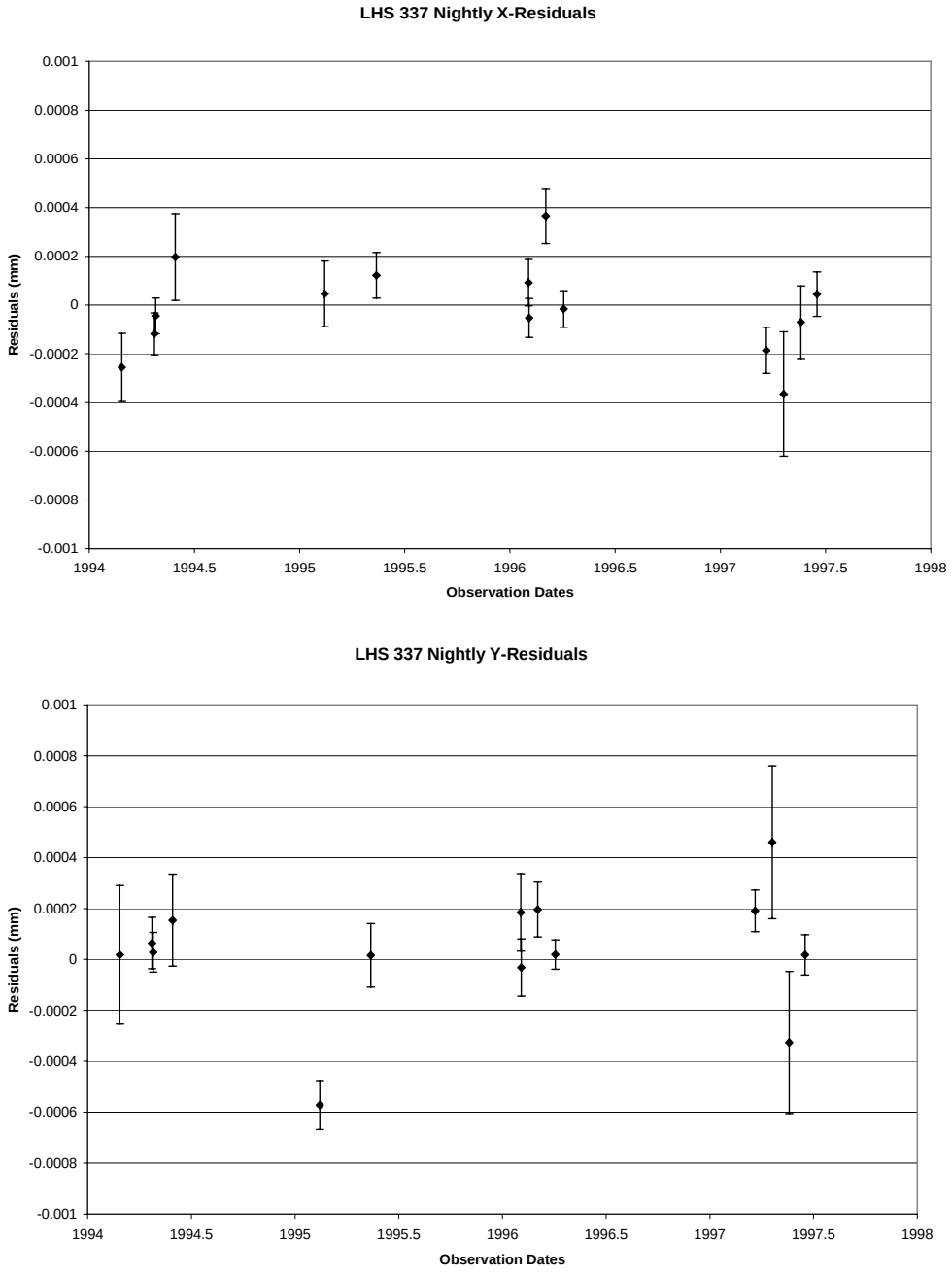

FIG. 3.11.—Nightly X- and Y-Residuals for LHS 337. Top chart contains x-residuals averaged by night. Bottom chart contains y-residuals averaged by night.

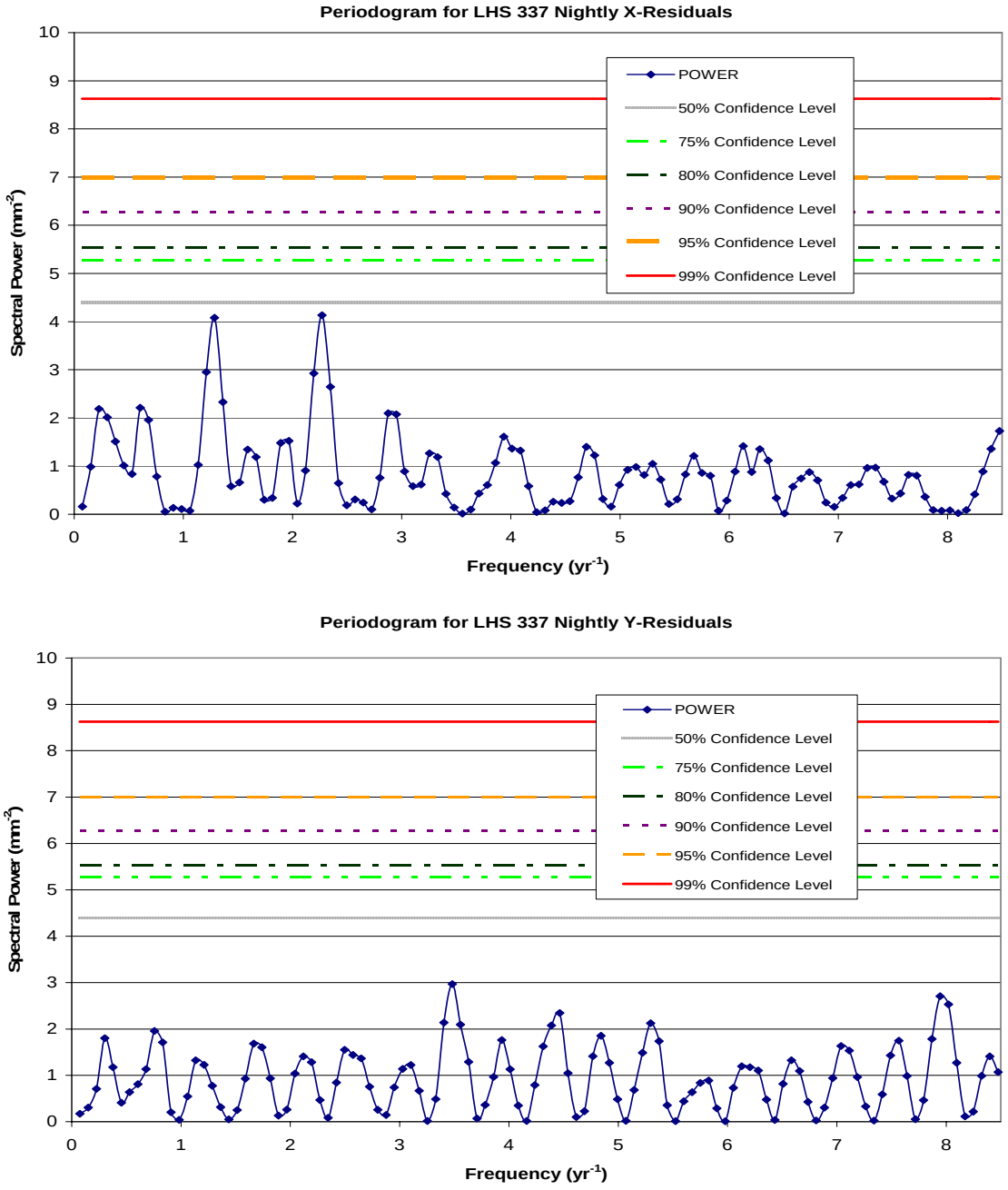

FIG. 3.12.—LHS 337 Periodograms. Top chart is a periodogram calculated for nightly x-residuals. Bottom chart is a periodogram calculated for nightly y-residuals. Horizontal lines in the periodograms indicate likelihood that spectral peaks exceeding that power are real and not caused by noise only. Solid line is 99% confidence, dashed line 95% confidence, dotted line 90% confidence, dash dotted line is 80% confidence, dash double-dotted line is 75% confidence, and hashed line is 50% confidence.

TABLE 3.16
FEATURES OF PERIODOGRAMS FOR LHS 337

Feature	Frequency (yr^{-1})	Period (yr)	Power (mm^{-2})	False Alarm Probability (%)	Comment
All X, maximum	13.7	0.07	7.3	23	27-day period, monthly observing cycle?
All Y, maximum	58.3	0.02	6.5	47	6-day period
Nightly X, maximum	2.3	0.44	4.1	60	
Nightly Y, maximum	3.5	0.29	3.0	95	

3.2.2.5 LHS 532

LHS 532 is the faintest star in this study as shown in Table 3.4 and Table 3.6. DCR corrections were applied to LHS 532 and all its reference stars. Because of the questionable nature of one new frame, only 100 out of 101 frames produced useable residuals (P. Ianna 2006, private communication; M. Begam 2006, private communication).

As shown in Figure 3.13 and Figure 3.14, LHS 532 still shows no sign of any perturbation. According to section 3.2.3, this study could detect companions more massive than 6 ± 1 M_{24}. Although a strong local peak in the periodogram for all x-residuals at 2.9 yr^{-1}, which corresponds to a 0.35-year period, matches the highest peak in the nightly x-residual periodogram, the nightly residual maximum has a 77% false alarm probability making these features mostly noise-related. In addition, neither of the y-residual periodograms have any points with even a 50% chance of being real. Table 3.17 lists the features of the periodograms for LHS 532.

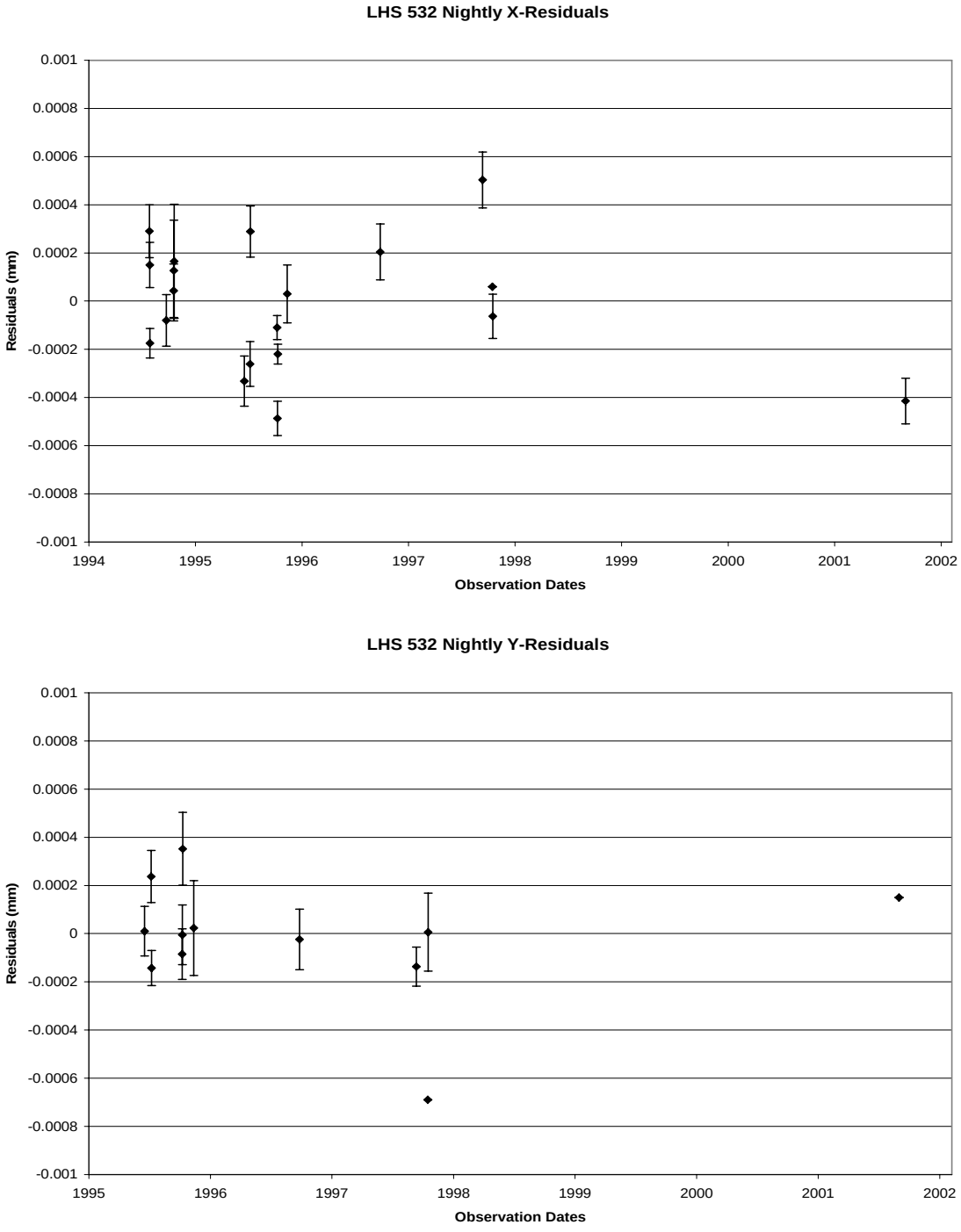

FIG. 3.13.— Nightly X- and Y-Residuals for LHS 532. Top chart contains x-residuals averaged by night. Bottom chart contains y-residuals averaged by night.

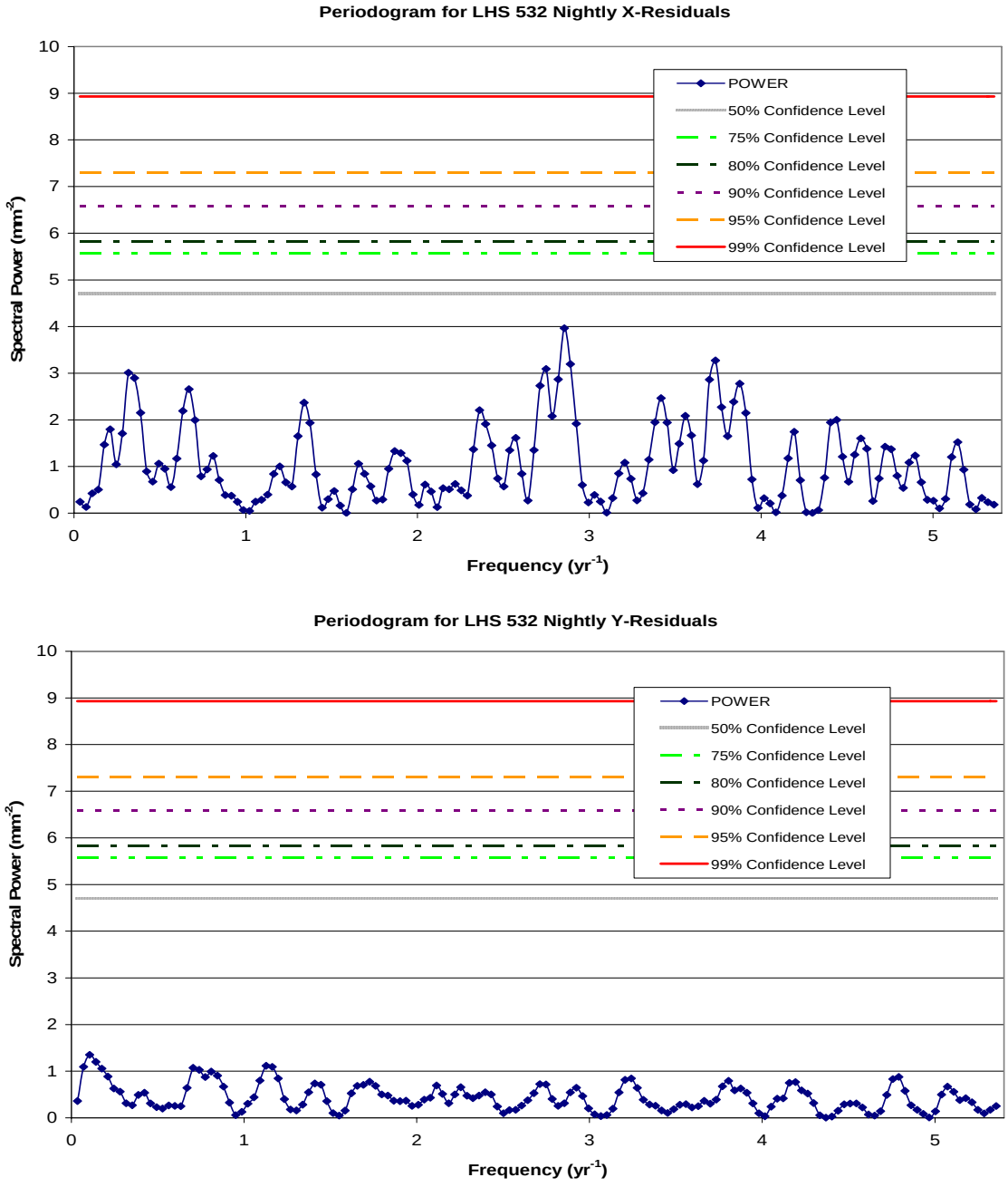

FIG. 3.14.— LHS 532 Periodograms. Top chart is a periodogram calculated for nightly x-residuals. Bottom chart is a periodogram calculated for nightly y-residuals. Horizontal lines in the periodograms indicate likelihood that spectral peaks exceeding that power are real and not caused by noise only. Solid line is 99% confidence, dashed line 95% confidence, dotted line 90% confidence, dash dotted line is 80% confidence, dash double-dotted line is 75% confidence, and hashed line is 50% confidence.

TABLE 3.17
FEATURES OF PERIODOGRAMS FOR LHS 532

Feature	Frequency (yr^{-1})	Period (yr)	Power (mm^{-2})	False Alarm Probability (%)	Comment
All X, maximum	7.0	0.14	14.2	<1	
All X, local peak	2.9	0.35	11.0	<1	matches maximum in nightly x
All Y, maximum	22.2	0.05	3.2	>99	
Nightly X, maximum	2.9	0.35	4.0	77	corresponds to local peak in all x
Nightly Y, maximum	0.1	9.46	1.3	>99	

3.2.2.6 LHS 1134

With fifty-one images taken on twelve nights, LHS 1134 has fewest of both spread over a 6-year baseline. Despite the paucity of exposures, the relative parallax calculated for LHS 1134 has an error less than 2.5 mas but it is the second largest such error in this study. The associated mean errors of unit weight are less than 0.5 μm and fall near the median value for this study. DCR corrections were not applied to LHS 1134 and its reference stars as noted in Table 3.7. LHS 1134 was observed using the R_C filter so DCR may be significant for the five frames that were taken at high hour angles.

During the preliminary analysis, no hint of a perturbation or any interesting features in the periodograms were noted. As shown in Figure 3.15 and Figure 3.16, LHS 1134 continues to show no sign of any periodic motion due to companions more massive than 7 ± 1 $M_{2\downarrow}$ as discussed in section 3.2.3. The maxima in both y-residual periodograms occur at 1.1 yr^{-1}, which corresponds to a 0.92-year period but the nightly residual maximum has a 73% false alarm probability making these features mostly noise-related. In addition, neither of the x-residual periodograms have any points with even a 50% chance of being real. Table 3.18 lists the features of the periodograms for LHS 1134.

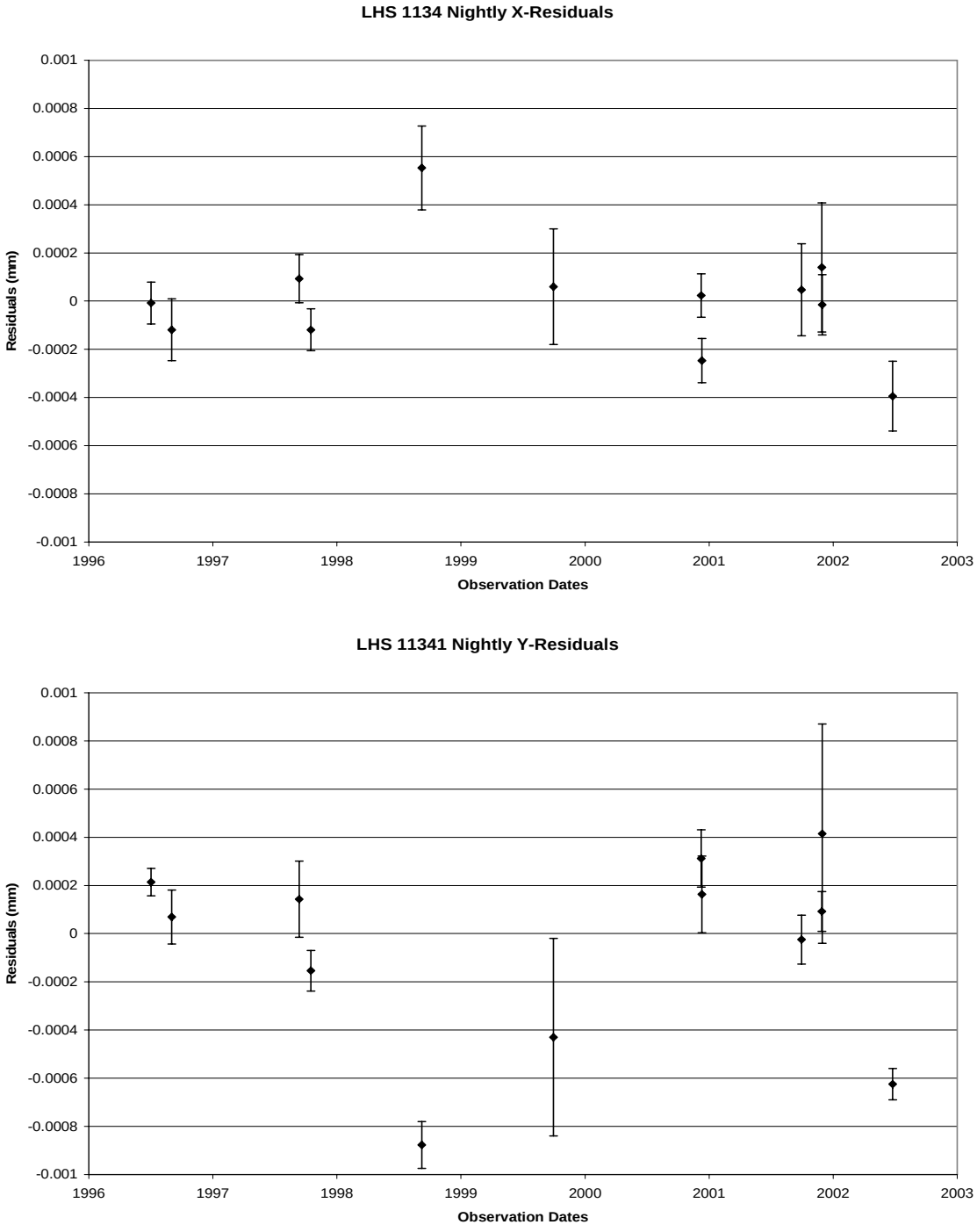

FIG. 3.15.— Nightly X- and Y-Residuals for LHS 1134. Top chart contains x-residuals averaged by night. Bottom chart contains y-residuals averaged by night.

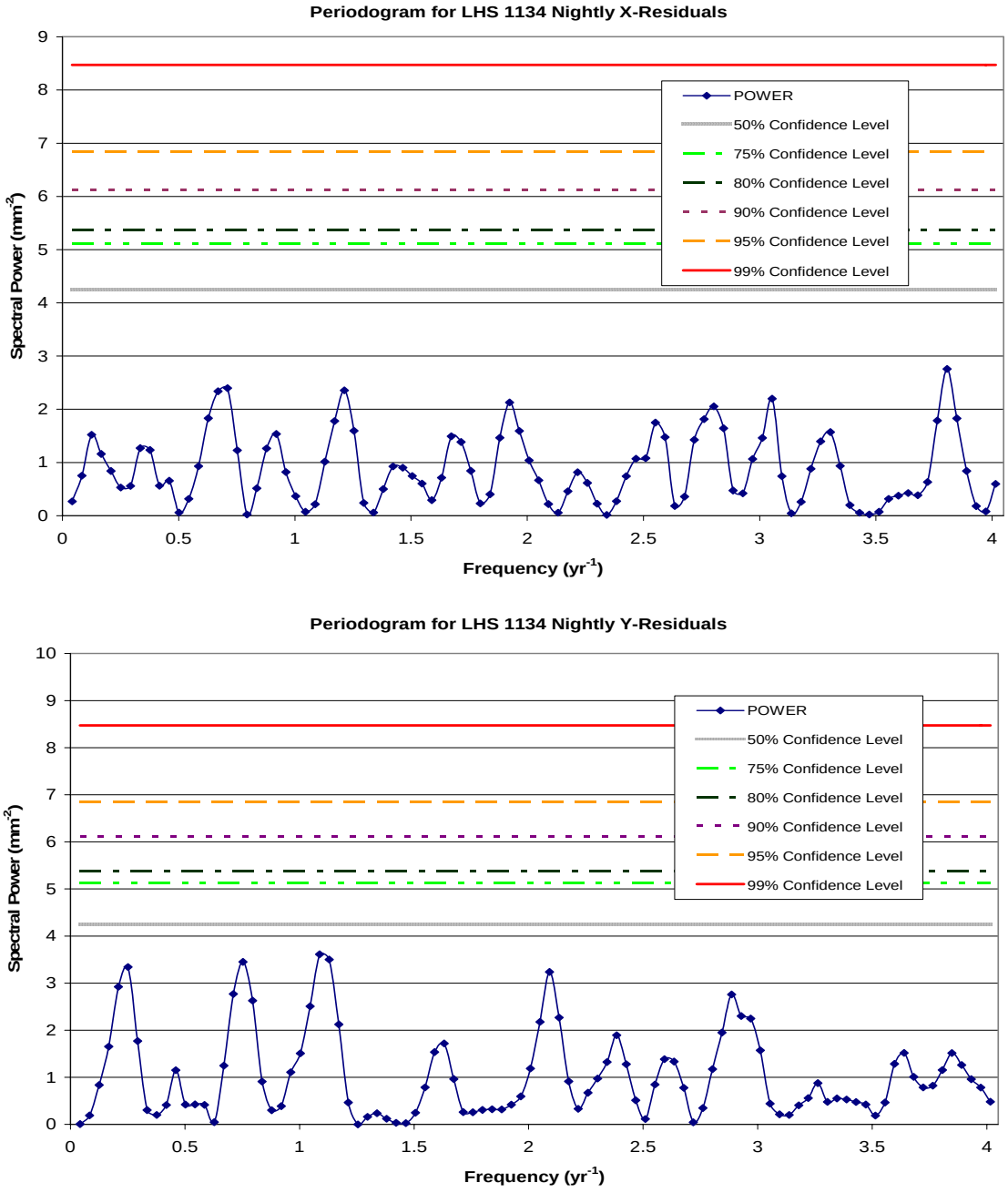

FIG. 3.16.— LHS 1134 Periodograms. Top chart is a periodogram calculated for nightly x-residuals. Bottom chart is a periodogram calculated for nightly y-residuals. Horizontal lines in the periodograms indicate likelihood that spectral peaks exceeding that power are real and not caused by noise only. Solid line is 99% confidence, dashed line 95% confidence, dotted line 90% confidence, dash dotted line is 80% confidence, dash double-dotted line is 75% confidence, and hashed line is 50% confidence.

TABLE 3.18
FEATURES OF PERIODOGRAMS FOR LHS 1134

Feature	Frequency (yr^{-1})	Period (yr)	Power (mm^{-2})	False Alarm Probability (%)	Comment
All X, maximum	17.0	0.06	4.4	91	
All Y, maximum	1.1	0.92	8.3	5	matches maximum in nightly y
Nightly X, maximum	3.8	0.26	2.8	96	
Nightly Y, maximum	1.1	0.92	3.6	73	matches maximum in all y

3.2.2.7 LHS 1565

LHS 1565 is the nearest star in this study. The photographic SPP previously measured a preliminary absolute parallax of 273 ± 5 mas, which put it at a distance of 3.7 pc (Ianna 1997) and ranked it twentieth among the nearest star systems (Henry *et al*. 1997). It also has the latest spectral type of the main sequence stars in this study, M5.5 V (Henry *et al*. 1997), which it shares with LHS 288.

As shown in Figure 3.1, LHS 1565, like LHS 337, served as an example of a star with no hint of perturbation detected by the preliminary analysis. As explained in Table 3.7, no DCR correction was applied to LHS 1565 and its reference stars. LHS 1565 was observed using the V_C filter. Because photon count changes little for red stars in V-band, DCR is reduced (Jao *et al*. 2004). In addition, only 5% of the exposures for LHS 1565 were taken at large hour angles.

As shown in Figure 3.17 and Figure 3.18, LHS 1565 still shows no sign of any perturbation by a planet more massive than 1.7 ± 0.4 M_{2J} as shown in section 3.2.2. Table 3.19 lists the features of the periodograms for LHS 1565. As in the preliminary periodograms, the highest peaks for all x- and y-residuals occurred at frequencies corresponding to periods of less than two months with false alarm possibilities less than 10%. The pattern of observations makes such short periods unlikely to be real; neither frequency was sampled when the individual residuals are combined as nightly normal

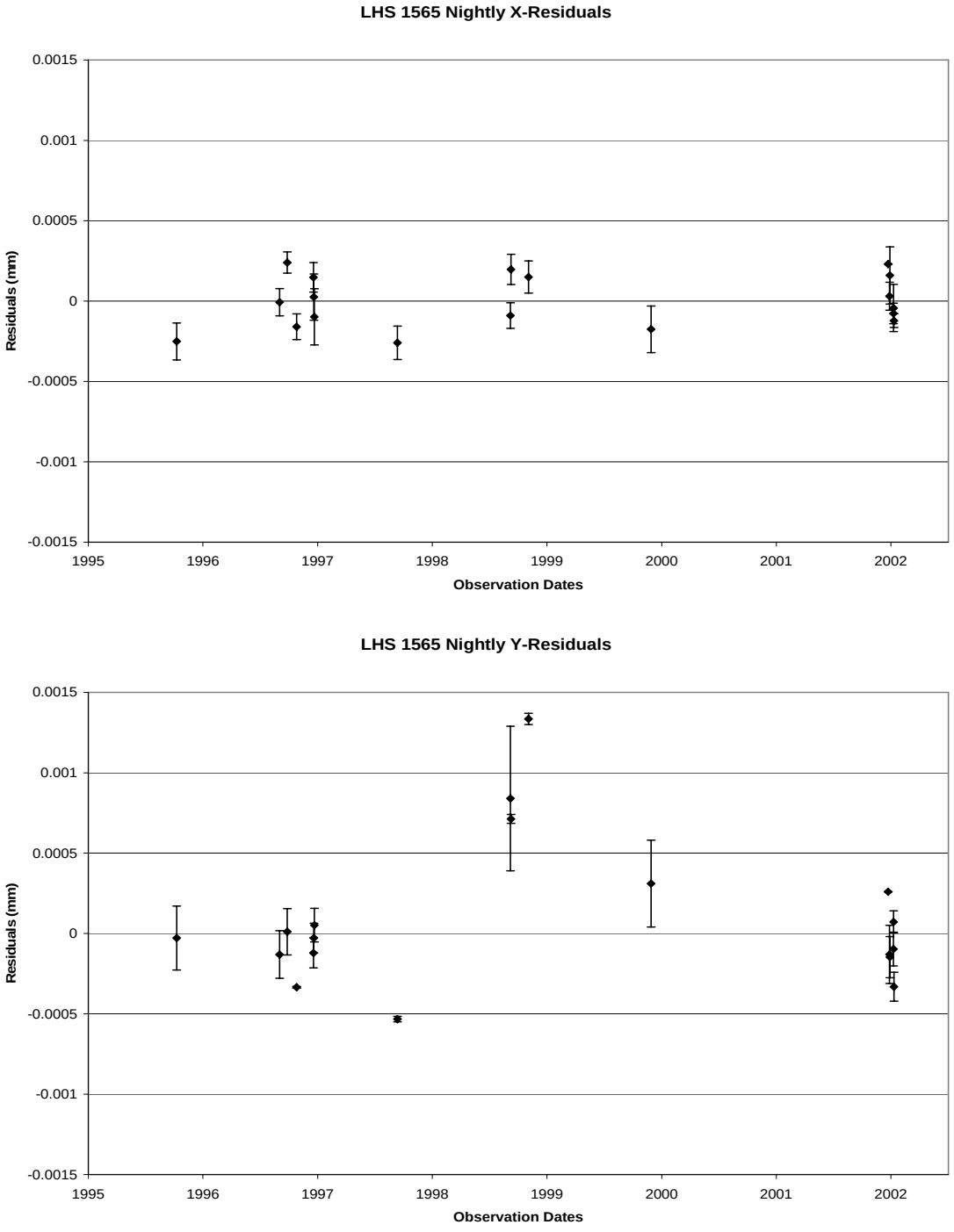

FIG. 3.17.— Nightly X- and Y-Residuals for LHS 1565. Top chart contains x-residuals averaged by night. Bottom chart contains y-residuals averaged by night.

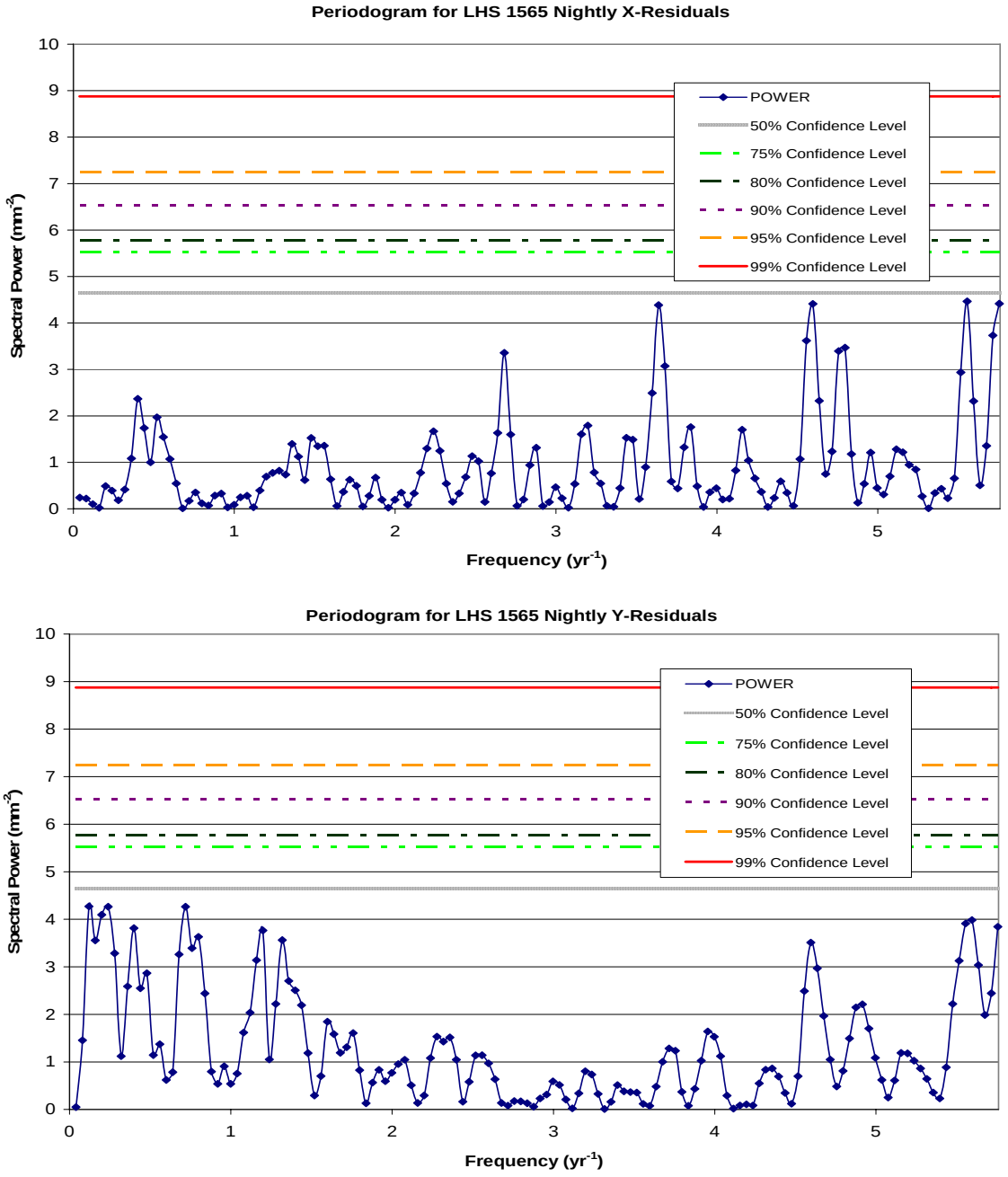

FIG. 3.18.— LHS 1565 Periodograms. Top chart is a periodogram calculated for nightly x-residuals. Bottom chart is a periodogram calculated for nightly y-residuals. Horizontal lines in the periodograms indicate likelihood that spectral peaks exceeding that power are real and not caused by noise only. Solid line is 99% confidence, dashed line 95% confidence, dotted line 90% confidence, dash dotted line is 80% confidence, dash double-dotted line is 75% confidence, and hashed line is 50% confidence.

TABLE 3.19
FEATURES OF PERIODOGRAMS FOR LHS 1565

Feature	Frequency (yr^{-1})	Period (yr)	Power (mm^{-2})	False Alarm Probability (%)	Comment
All X, maximum	9.911	0.1009	8.814	5	frequency too high for nightly residuals
All X, local peak	0.1599	6.255	1.293	>50	adjacent to frequency of interest
All X, adjacent to local peak	0.1199	8.340	0.7255	>50	corresponds to maximum in nightly y
All X, local peak	5.555	0.1800	7.007	<50	corresponds to maximum in nightly x
All Y, maximum	6.754	0.1481	8.237	8	frequency too high for nightly residuals
All Y, local peak	0.1199	8.340	7.390	<20	corresponds to maximum in nightly y
All Y, local peak	5.595	0.1787	6.526	<50	adjacent to frequency of interest
All Y, adjacent to local peak	5.555	0.1800	5.624	>50	corresponds to maximum in nightly x
Nightly X, maximum	5.555	0.1800	4.464	57	corresponds to local peak in all x
Nightly X	0.1199	8.340	0.09870	>50	corresponds to maximum in nightly y
Nightly Y, maximum	0.1199	8.340	4.272	64	corresponds to local peak in all y

points. When the residuals were combined into nightly normal points, the periodograms show no peaks that had as much as a 50% chance of being real.

3.2.2.8 LHS 2310

LHS 2310 has the smallest proper motion of any star in this study. Although it has the largest error in parallax and largest unit error of mean weight in x, the overall quality of its parallax and proper motion solution along with its 6.7-year baseline was sufficient to ensure its inclusion in the second sample. In computing the relative parallax and proper motion of LHS 2310, 114 images taken on 20 nights between 1994 April and 2001 January were used. Because of the questionable nature of one exposure, only 113 frames were used to determine the parallax and proper motion of LHS 2310. The observations were made exclusively with CCD #6.

As explained in Table 3.7, no DCR correction was available for LHS 2310 and its reference stars, which were observed using the R_C filter. Although significant DCR might be expected for a red star observed in R-band (Jao *et al*. 2005), only 8% of the exposures used were taken at large hour angles.

At best, Figure 3.19 and Figure 3.20 hint of a 3.0 to 3.4-year period perturbation in LHS 2310. According to section 3.2.3, this study could detect brown dwarfs more massive than $16 \pm 2\ M_{24}$. The maxima for all y- and nightly y-residuals occur at the same frequency, 3.7 yr^{-1}, which corresponds to a period of approximately 99 days but no matching peaks occur in either x-periodogram. The periodograms for nightly residuals have no points with a 50% or greater likelihood of begin real. Table 3.20 lists the features of the periodograms for LHS 2310.

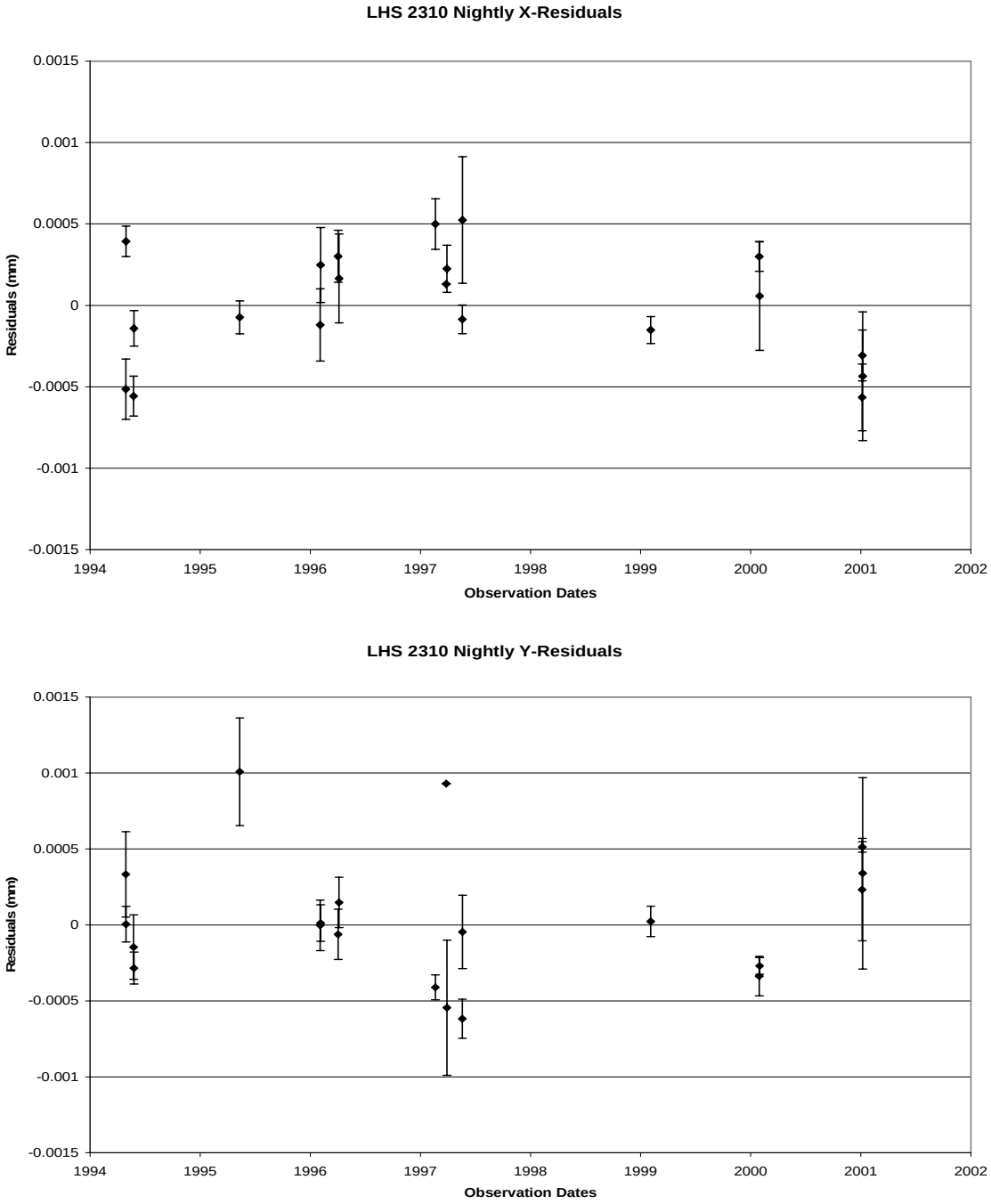

FIG. 3.19.— Nightly X- and Y-Residuals for LHS 2310. Top chart contains x-residuals averaged by night. Bottom chart contains y-residuals averaged by night.

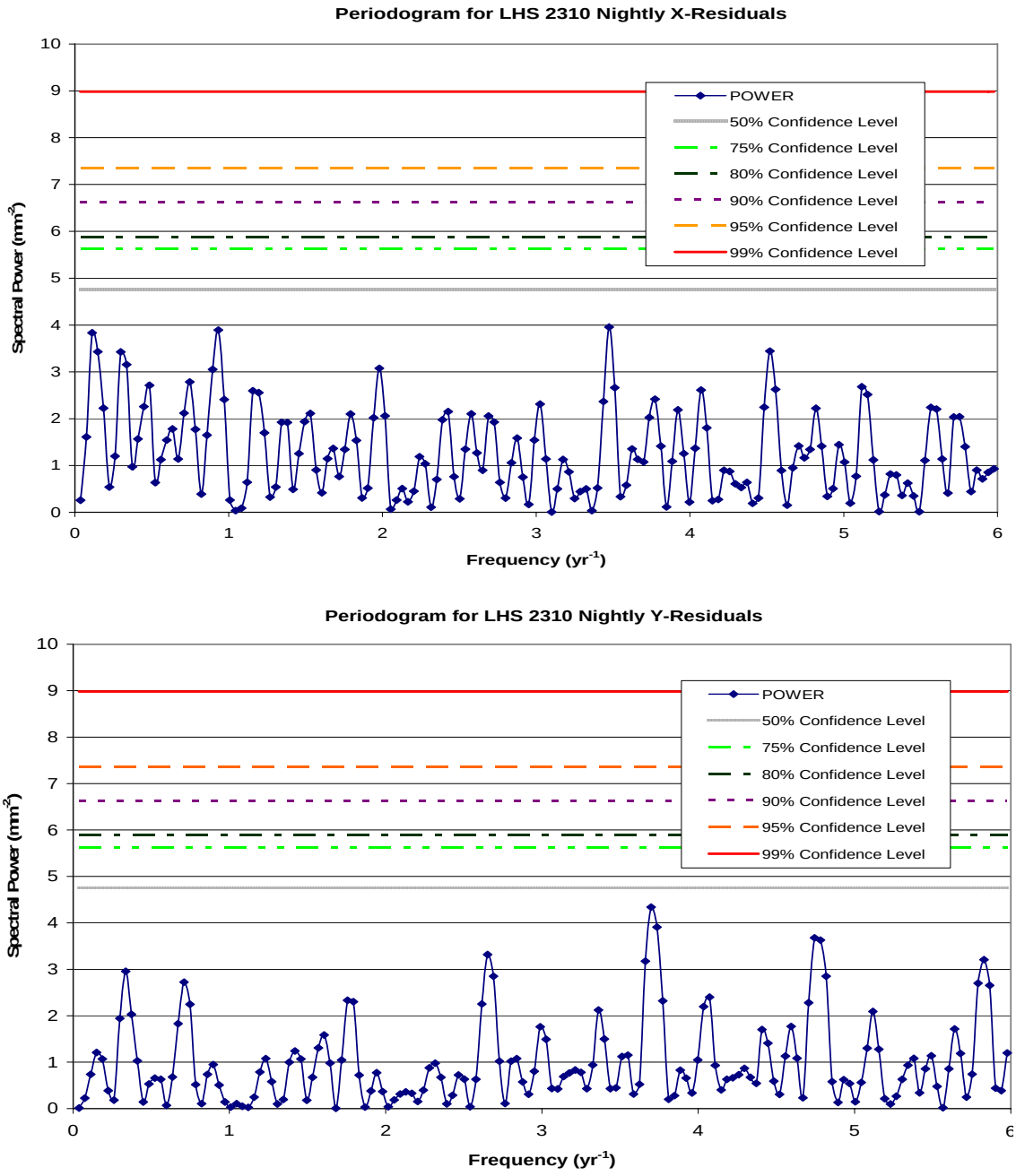

FIG. 3.20.— LHS 2310 Periodograms. Top chart is a periodogram calculated for nightly x-residuals. Bottom chart is a periodogram calculated for nightly y-residuals. Horizontal lines in the periodograms indicate likelihood that spectral peaks exceeding that power are real and not caused by noise only. Solid line is 99% confidence, dashed line 95% confidence, dotted line 90% confidence, dash dotted line is 80% confidence, dash double-dotted line is 75% confidence, and hashed line is 50% confidence.

TABLE 3.20
FEATURES OF PERIODOGRAMS FOR LHS 2310

Feature	Frequency (yr^{-1})	Period (yr)	Power (mm^{-2})	False Alarm Probability (%)	Comment
All X, maximum	27.2	0.04	14.4	<1	
All X, local peak	0.3	3.35	7.5	<25	possible corresponding signal in all y
All Y, maximum	3.7	0.27	11.4	1	matches maximum in nightly y
All Y, adjacent to local peak	0.3	3.35	6.7	<50	corresponds to local peak in all x
All Y, local peak	0.3	2.97	7.7	<20	adjacent to interesting frequency in all x and y
Nightly X, maximum	3.5	0.29	4.0	79	
Nightly Y, maximum	3.7	0.27	4.3	65	matches maximum in all y

3.2.2.9 LHS 2739

LHS 2739 is the most distant star in this study; its relative parallax places it at a distance of about 23 parsecs. LHS 2739 benefits from the largest number of images available for a star in this study; it shares the smallest error in parallax of 0.9 mas with LHS 3418 and has the smallest mean error of unit weight in y. Between 1994 April and 2001 June, 140 useable observations were made of LHS 2739. Before calculating the final periodograms, DCR corrections were applied to LHS 2739 and its reference stars.

As shown in Table 3.7, the DCR correction for LHS 2739 suffered from two problems: no photometry for 3 out of 14 reference stars and no weather data for 30 out of 141 frames. The reference stars without photometry were assumed to have spectral type G0V. Because weather data were also unavailable on days adjacent to those observation dates without weather, weather from the same day in another year was used. LHS 2739 was observed using the R_C filter for which DCR can be significant. However, only ten frames were taken at large hour angles and the largest was less than 42 minutes west. In addition, the majority of frames were taken within 20 minutes of the meridian.

The preliminary analysis identified no interesting features in the periodograms calculated for LHS 2739. Figure 3.21 and Figure 3.22 indicate that LHS 2739 is without companions more massive than the limit of $17 \pm 2\ M_{2l}$ set in section 3.2.3 for this study. The maximum peak in the periodograms for nightly residuals has a greater than 50% chance of being real and has a corresponding local peak in all x-residuals.

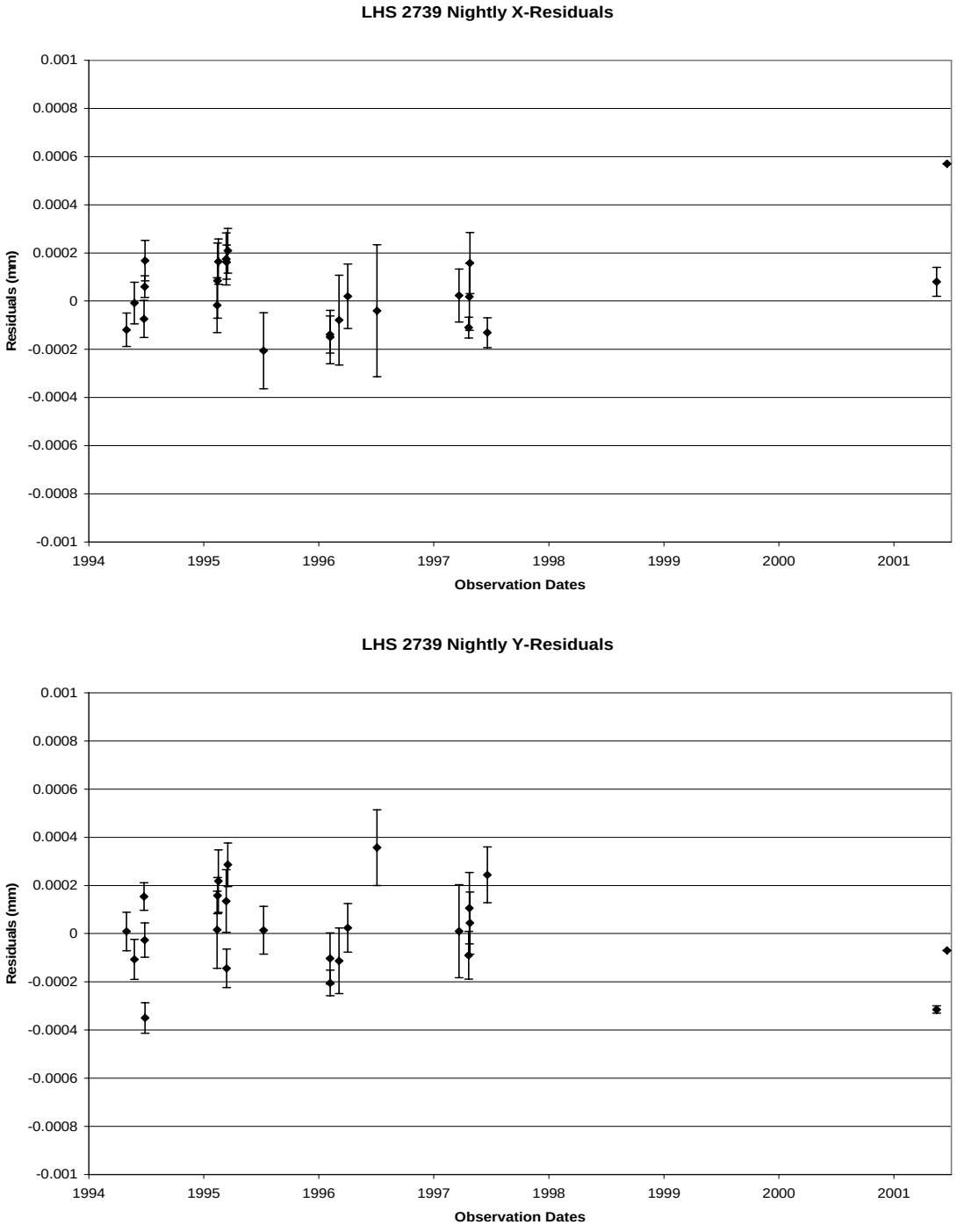

FIG. 3.21.— Nightly X- and Y-Residuals for LHS 2739. Top chart contains x-residuals averaged by night. Bottom chart contains y-residuals averaged by night.

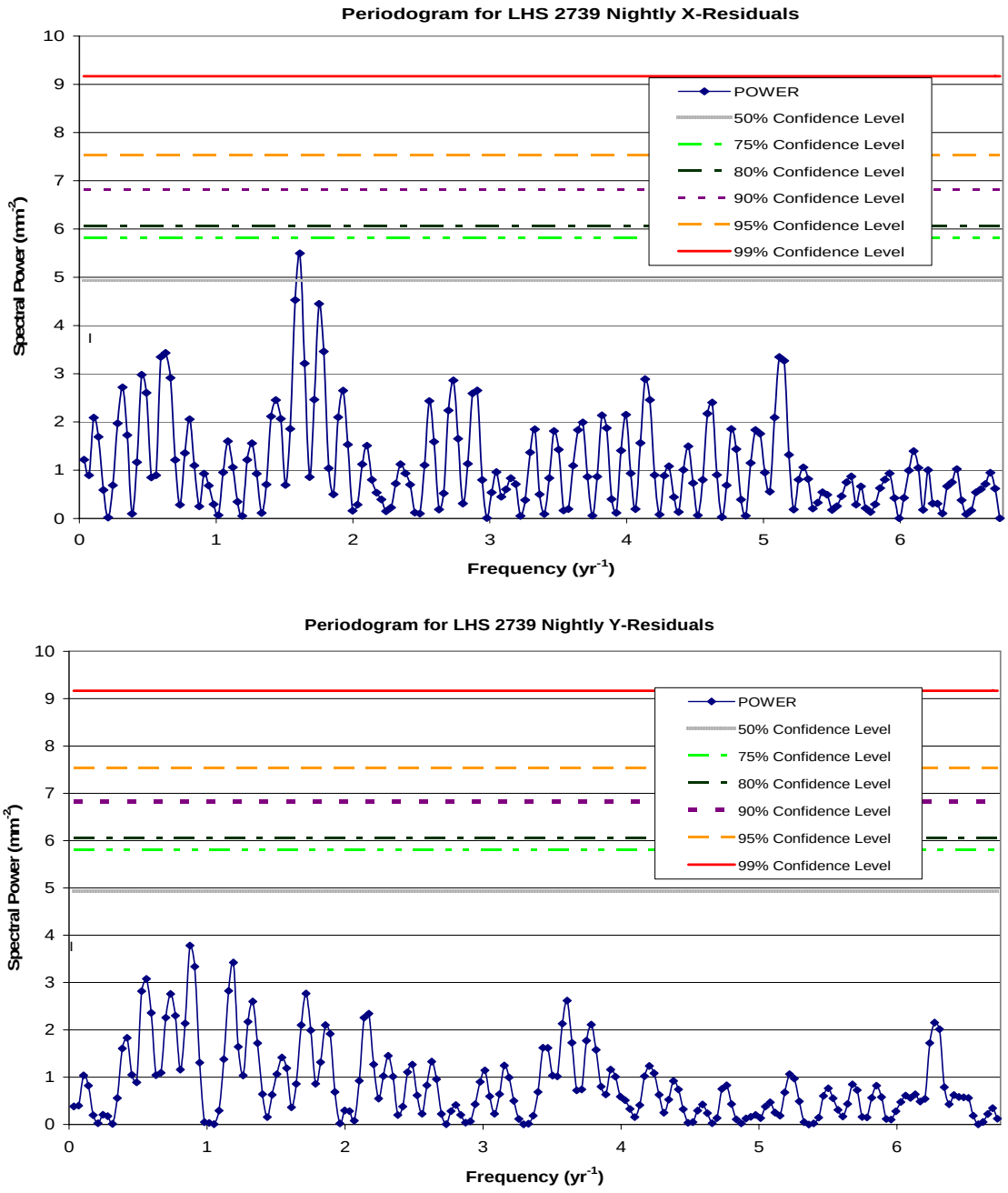

FIG. 3.22.—LHS 2739 Periodograms. Top chart is a periodogram calculated for nightly x-residuals. Bottom chart is a periodogram calculated for nightly y-residuals. Horizontal lines in the periodograms indicate likelihood that spectral peaks exceeding that power are real and not caused by noise only. Solid line is 99% confidence, dashed line 95% confidence, dotted line 90% confidence, dash dotted line is 80% confidence, dash double-dotted line is 75% confidence, and hashed line is 50% confidence.

TABLE 3.21
FEATURES OF PERIODOGRAMS FOR LHS 2739

Feature	Frequency (yr^{-1})	Period (yr)	Power (mm^{-2})	False Alarm Probability (%)	Comment
All X, maximum	14.1	0.07	7.8	21	
All X, local peak	1.6	0.62	7.6	<25	corresponds to maximum in nightly x
All Y, maximum	35.5	0.03	11.6	1	
All Y, local peak	0.9	1.14	7.4	<50	corresponds to maximum in nightly y
Nightly X, maximum	1.6	0.62	5.5	33	corresponds to local peak in all x
Nightly Y, maximum	0.9	1.14	3.8	89	corresponds to local peak in all y

These peaks occur at a frequency of 1.6 yr^{-1}, which corresponds to a period of approximately 227 days. The short period represented and the lack of corresponding signals in the y-periodograms make noise the most likely origin of these peaks. The nightly y-residual maximum has a matching local peak in the periodogram for all y-residuals. These peaks occur at a frequency of 0.9 yr^{-1}, which corresponds to a period of approximately 1.14 year. Table 3.21 summarizes these features.

3.2.2.10 LHS 2813

LHS 2813 was the star with the most promising periodograms during the preliminary analysis, which covered observations made between 1994 and mid-1997. It is one of the more distant stars in this study at about 17 pc. It also has the second smallest proper motion in Table 3.5 based on slightly more than eight years of observations (BIP). It is also a relatively early red dwarf with spectral type M2.0 V (Hawley, Gizis, & Reid 1996).

Figure 3.1 shows local peaks that occur in all four periodograms at a frequency of 0.5293 yr^{-1}, which corresponds to a period of approximately 1.889 years. For the nightly x-residual periodogram, this peak is also the maximum but one with less than 50% chance of being real. For the y-periodograms, these local peaks are weak; both have less than a 50% chance of being real. Although a companion might be expected to produce signals of similar strength in both coordinates, some orientations would produce a signal primarily in the x-coordinate. Although the potential signal at this frequency is probably due to noise, it was worth further investigation.

After the preliminary analysis, five more observations taken in 2002 were added to the calculation of relative parallax and proper motion calculation for LHS 2813. Then, all the observations were corrected for DCR. The resulting pif was found to have frames that appeared to be out of order; this temporal discontinuity was corrected as discussed in 3.2.1. The results of these updated calculations are shown in Figure 3.23 and Figure 3.24.

In the final periodograms, the situation for LHS 2813 is less clear. The maxima for the y-residual periodograms have moved to 0.5208 yr^{-1}, which corresponds to a period of approximately 1.920 years—close to the earlier period of interest. However, the maxima for the x-residual periodograms both have moved away from the earlier frequency of interest to a frequency of 0.3676 yr^{-1}, which corresponds to a period of approximately 2.720 years. The new maximum in the nightly x-residual periodogram has a false alarm probability of only 14%. The all x-residual periodogram retains high power near the earlier frequency of interest but no peak occurs there or adjacent to that frequency. The nightly x-residual periodogram has a local peak adjacent to the earlier frequency of interest but it is a weak one with a less than 50% chance of being real. The all y-residual periodogram point that corresponds to the new maxima in the x-residual periodograms is adjacent to a local peak and has a greater than 50% chance of being real. In the nightly y-residuals, the frequency corresponding to the new maximum in the x-residual periodograms is adjacent to a weak local peak with a less than 50% chance of being real.

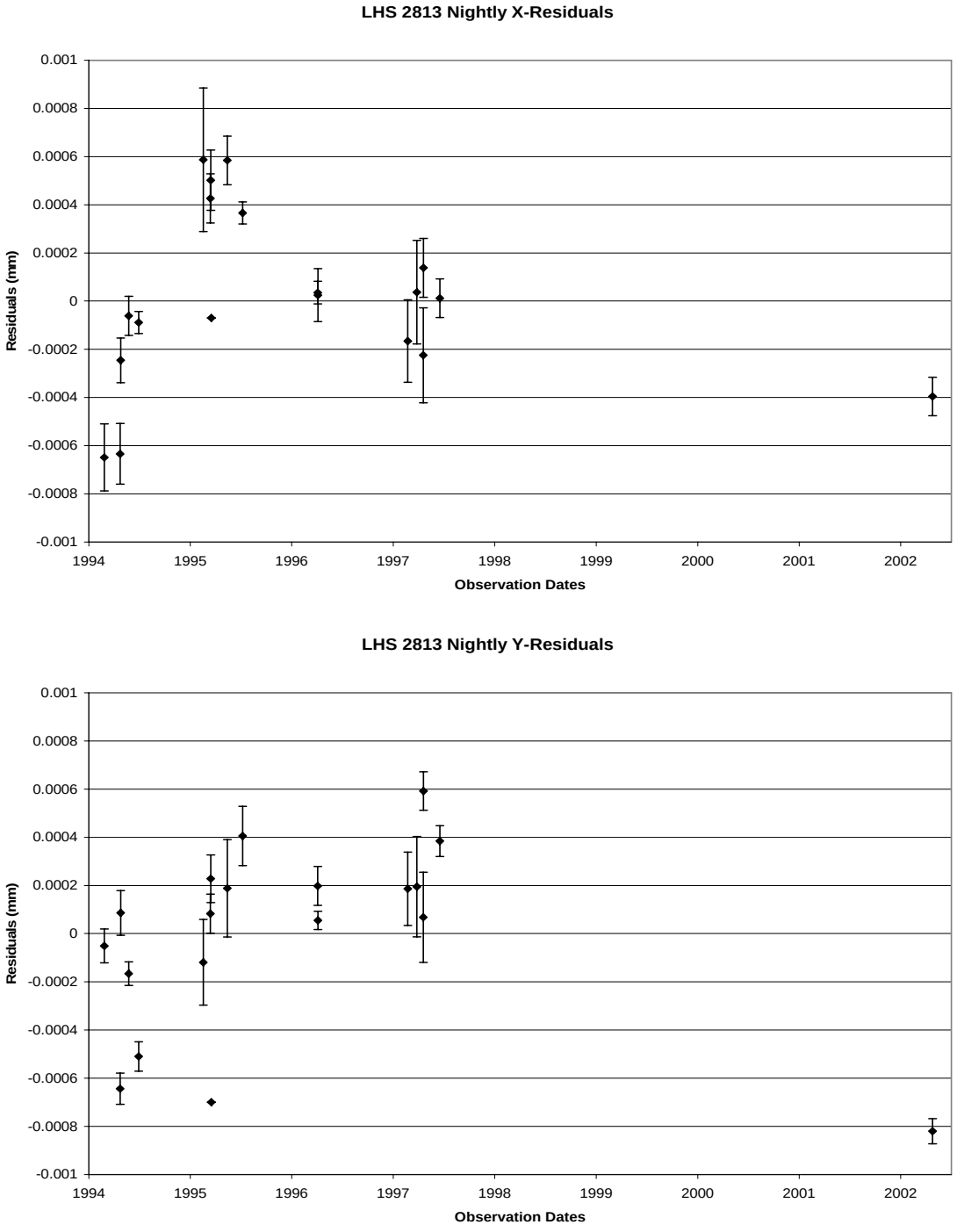

FIG. 3.23.—Nightly X- and Y-Residuals for LHS 2813. Top chart contains x-residuals averaged by night. Bottom chart contains y-residuals averaged by night.

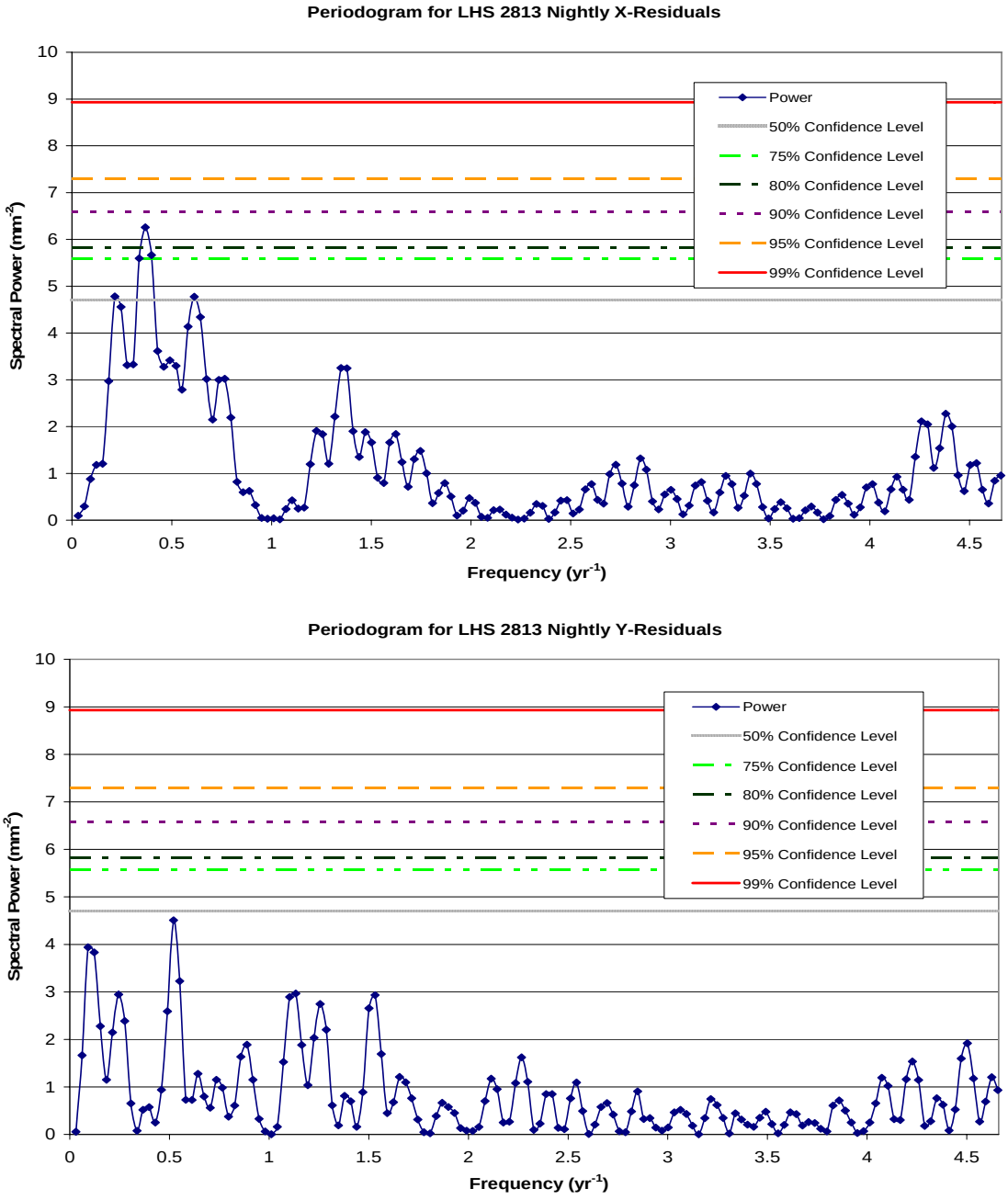

FIG. 3.24.—LHS 2813 Periodograms. Top chart is a periodogram calculated for nightly x-residuals. Bottom chart is a periodogram calculated for nightly y-residuals. Horizontal lines in the periodograms indicate likelihood that spectral peaks exceeding that power are real and not caused by noise only. Solid line is 99% confidence, dashed line 95% confidence, dotted line 90% confidence, dash dotted line is 80% confidence, dash double-dotted line is 75% confidence, and hashed line is 50% confidence.

TABLE 3.22
FEATURES OF PERIODOGRAMS FOR LHS 2813

Feature	Frequency (yr^{-1})	Period (yr)	Power (mm^{-2})	False Alarm Probability (%)	Comment
All X, maximum	0.36760	2.7204	30.033	<1	matches maximum in nightly x
All X, high power but no peak	0.52076	1.9203	18.661	<1	corresponds to maxima in both y
All Y, maximum	0.52076	1.9203	24.252	<1	matches maximum in nightly y
All Y, local peak	0.39823	2.5111	7.6087	<25	adjacent to frequency of interest (x maxima)
All Y, adjacent to local peak	0.36760	2.7204	7.3540	<50	corresponds to maxima in both x
Nightly X, maximum	0.3676	2.720	6.259	14	matches maximum in all x
Nightly X, local peak	0.4901	2.040	3.417	>50	adjacent to frequency of interest (y maxima)
Nightly X, adjacent to local peak	0.5208	1.920	3.297	>50	corresponds to maxima in both y
Nightly Y, maximum	0.5208	1.920	4.508	57	matches maximum in all y
Nightly Y, local peak	0.3982	2.511	0.5745	>50	adjacent to frequency of interest (x maxima)
Nightly Y, adjacent to local peak	0.3676	2.720	0.5168	>50	corresponds to maxima in both x

NOTE.—Preliminary study found possible perturbation with frequency of 0.5293 yr^{-1} or a period of about 1.889 years; the potential signal was more distinct in the x-residuals than the y-residuals.

The 8.16-year baseline for LHS 2813 is more than twice either period of interest, the frequencies of interest are both greater than the lowest independent frequency and less than the Nyquist frequency. Table 3.22 summarizes the features discussed. Brown dwarf companions more massive than 17 ± 2 M_{2J} should have been detectable by this study according to section 3.2.3. Although the weak signals identified here are most likely spurious, additional observations of LHS 2813 in a future study could further clarify the situation.

3.2.2.11 LHS 3064

LHS 3064 is a modest M3 star (Bidelman 1985) with the median apparent brightness (V_J) for this study and a relative parallax and proper motion close to the median values, as shown in Table 3.4 and Table 3.5. The preliminary periodograms for LHS 3064 contained no interesting features. Before the final reduction, an additional six observations made in 2001 and 2002 were included in the relative parallax and proper motion calculations for LHS 3064. Its final baseline was longer than eight years. The LHS 3064 pif appeared to have several frames out of order; this temporal discontinuity was corrected as discussed in 3.2.1. In addition, DCR corrections were applied to LHS 3064 and its reference stars.

After the additional frames were added and DCR corrections made, LHS 3064 still shows no sign of a perturbation, as displayed in Figure 3.25 and Figure 3.26. According to section 3.2.3, perturbations due to companions more massive than 6 ± 1 M_{2J} should have been revealed. The maxima in the all x- and all y-residual periodograms occur at very high frequencies, which are unlikely to be real. The

frequency in the all y-residual periodogram that corresponds to the maximum of the all x-residual periodogram is adjacent to a weak local peak. The maximum in the nightly x-residual periodogram has a less than 50% chance of being real as do the corresponding frequencies in the other three periodograms. The maximum in the nightly y-residual periodogram occurs at frequency of 1.99 yr^{-1}, which corresponds to a period of approximately 0.502 years; it has a less than 50% chance of being real. The corresponding frequency on all y-residual periodogram has a greater than 95% chance of being real and is adjacent to a local peak. The corresponding frequency on the nightly x-residual periodogram is a weak local peak with a less than 50% chance of being real. The semi-annual period may be a result of the parallax observing cycle, which requires images be taken in the mornings and evenings when the parallax factors are large. Table 3.23 lists the features of the LHS 3064 periodograms.

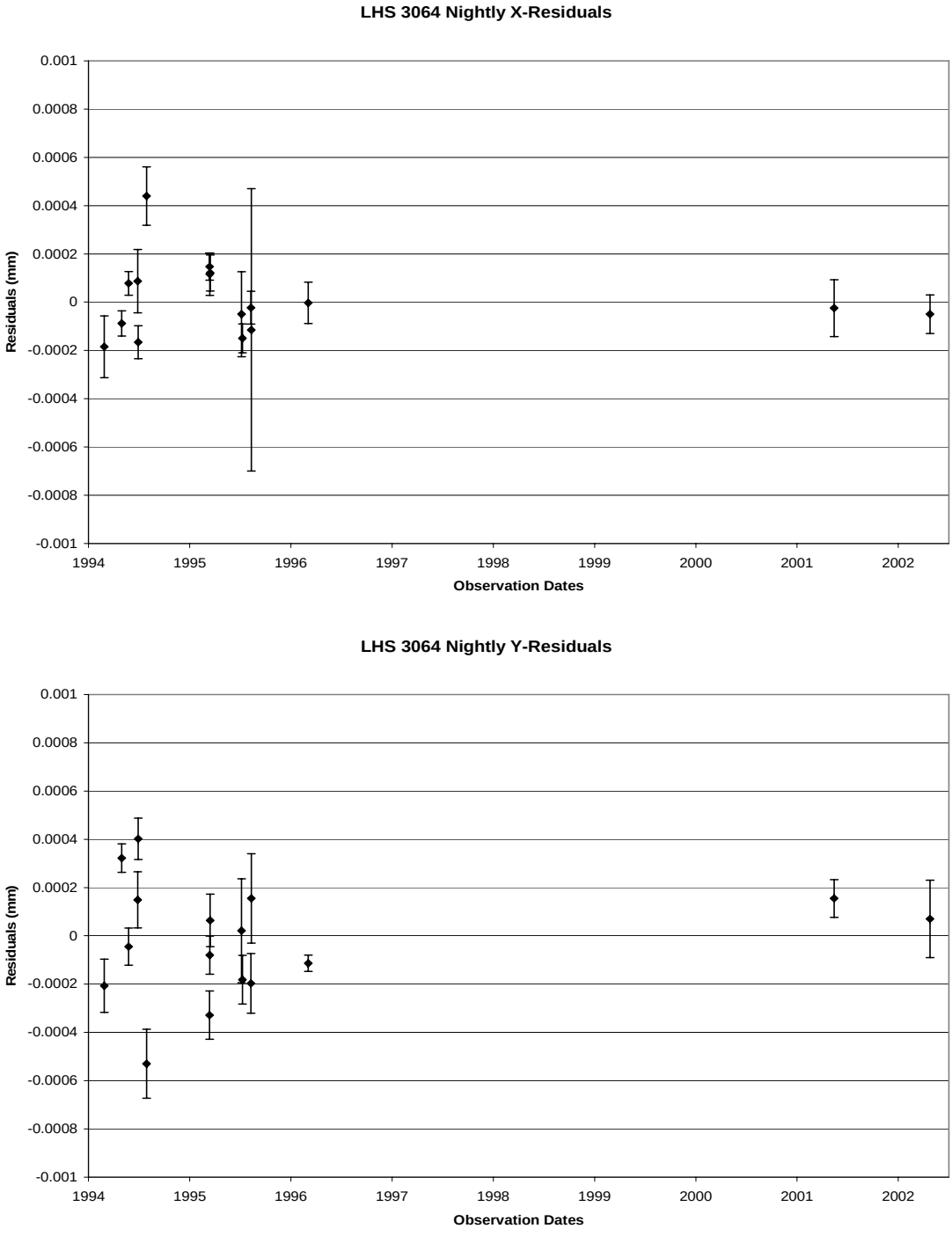

FIG. 3.25.— Nightly X- and Y-Residuals for LHS 3064. Top chart contains x-residuals averaged by night. Bottom chart contains y-residuals averaged by night.

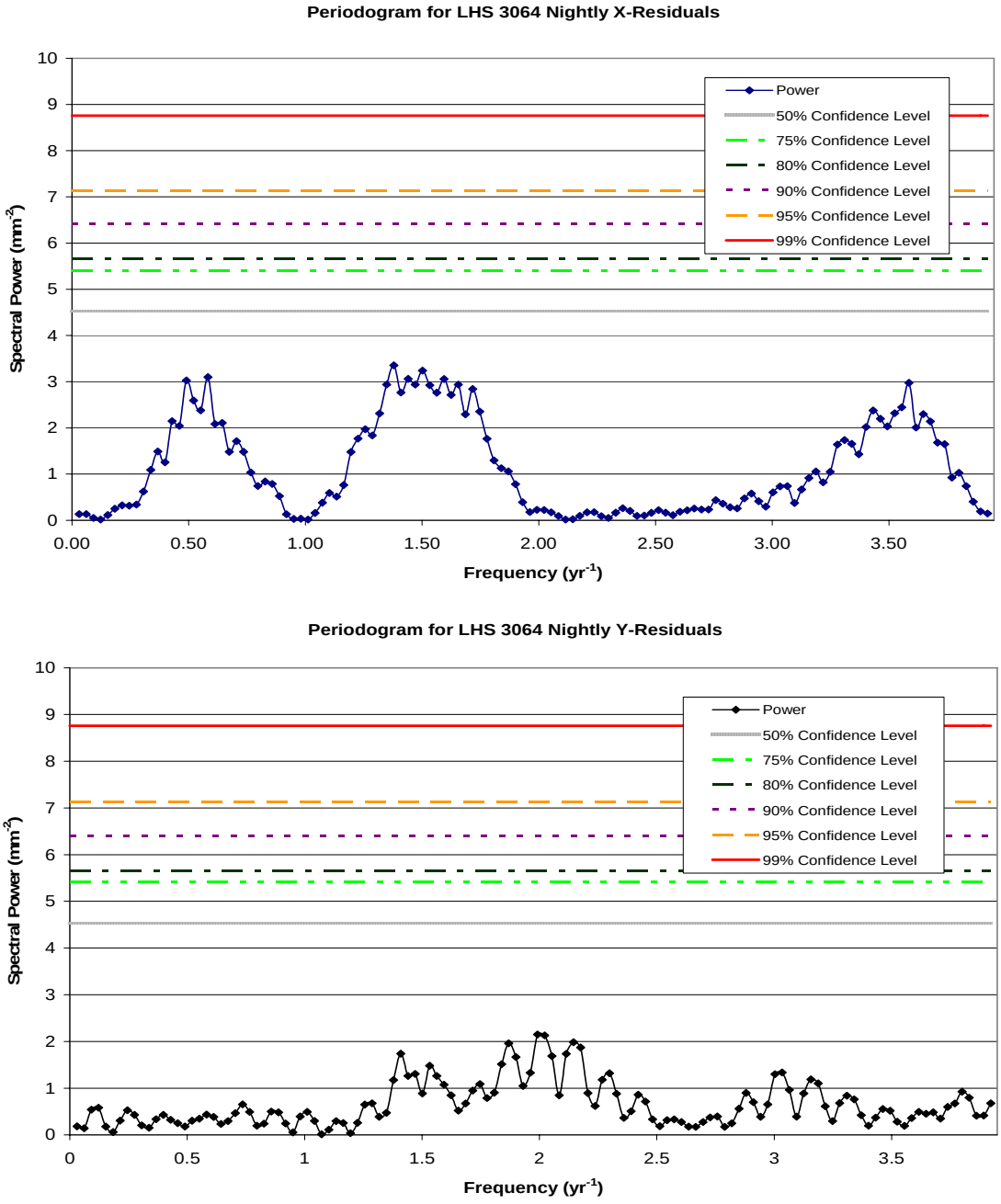

FIG. 3.26.— LHS 3064 Periodograms. Top chart is a periodogram calculated for nightly x-residuals. Bottom chart is a periodogram calculated for nightly y-residuals. Horizontal lines in the periodograms indicate likelihood that spectral peaks exceeding that power are real and not caused by noise only. Solid line is 99% confidence, dashed line 95% confidence, dotted line 90% confidence, dash dotted line is 80% confidence, dash double-dotted line is 75% confidence, and hashed line is 50% confidence.

TABLE 3.23
FEATURES OF PERIODOGRAMS FOR LHS 3064

Feature	Frequency (yr^{-1})	Period (yr)	Power (mm^{-2})	False Alarm Probability (%)	Comment
All X, maximum	11.062	0.090400	7.6433	21	~33 days, frequency too high for nightly residuals
All Y, maximum	19.182	0.052131	14.797	<1	~19 days, frequency too high for nightly residuals
All Y, local peak	2.0224	0.49446	10.058	<5	adjacent to frequency of interest (all y maximum)
All Y, adjacent to local peak	1.9918	0.50207	9.9274	<5	corresponds to maximum in nightly y
Nightly X, maximum	1.38	0.725	3.35	90	
Nightly X, local peak	1.99	0.502	0.228	>50	corresponds to maximum in nightly y
Nightly Y, maximum	1.99	0.502	2.15	<1	~6 months, probably related to observing cycle

3.2.2.12 LHS 3242

LHS 3242 is the brightest star in this study as shown in Table 3.4 and has the earliest spectral type of the main sequence stars, M0.5 V (Hawley, Gizis, & Reid 1996). The moderate errors associated with its relative parallax and a baseline longer than eight years contributed to its inclusion in the second sample.

Although DCR correction is not yet possible for LHS 3242 and its reference stars as explained in Table 3.7, only 2% of the exposures used were made at large hour angles. LHS 3242 was observed with the V_C filter; DCR is reduced because the photon count changes little for red stars across this passband (Jao *et al*. 2005).

The residuals after the calculation of relative parallax and proper motion for LHS 3242 are shown in Figure 3.27 along with their associated periodograms in Figure 3.28. No pattern that might indicate the presence of brown dwarf companions more massive than 18 ± 1 M_{24} is present; the minimum detectable companion mass is discussed in section 3.2.3. The maxima in the all x- and all y-residual periodograms occur at high frequencies that are not sampled when the data is averaged by night. No point on either nightly periodogram has a 50% or greater chance of being real. Table 3.24 lists the features of these periodograms.

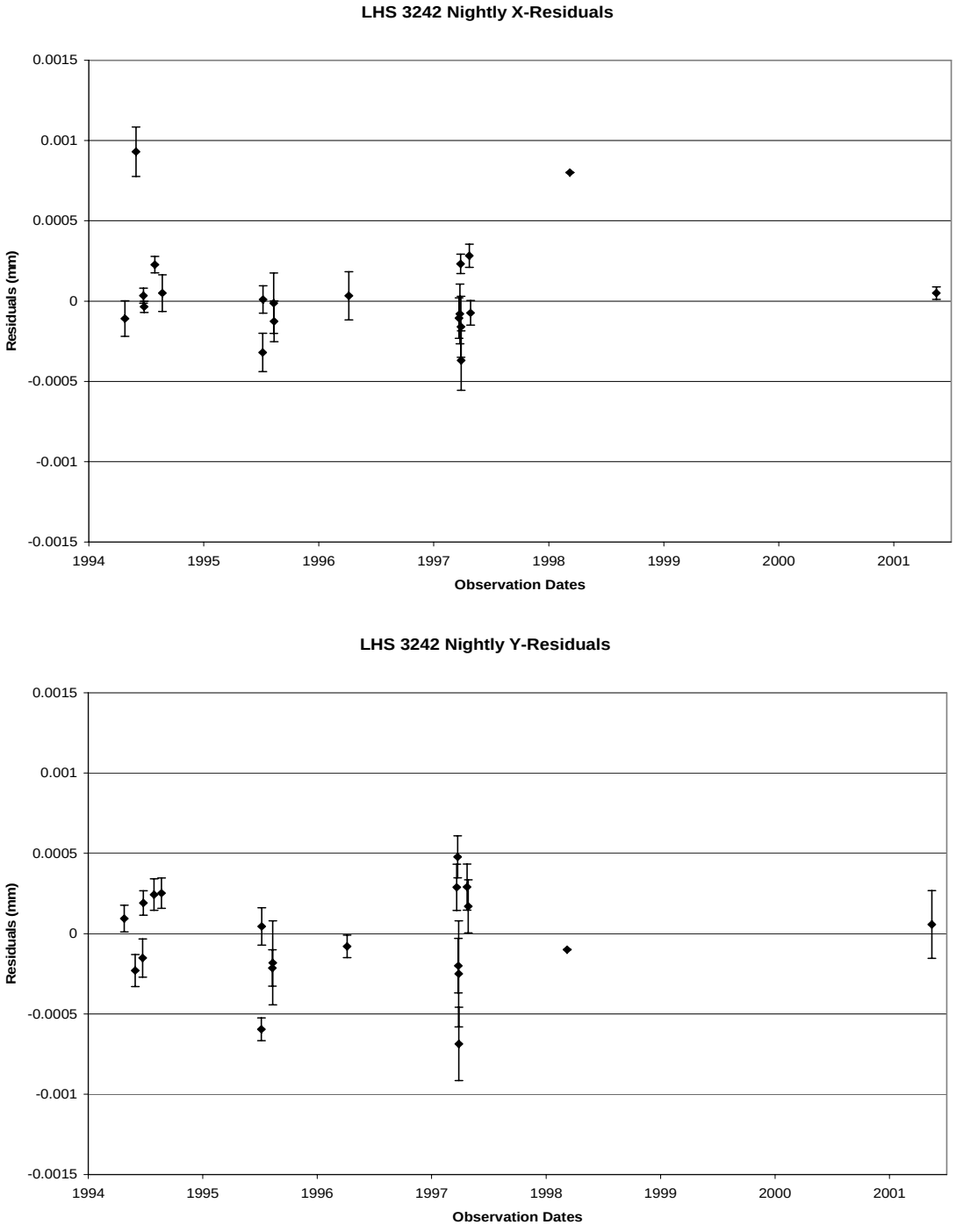

FIG. 3.27.—Nightly X- and Y-Residuals for LHS 3242. Top chart contains x-residuals averaged by night. Bottom chart contains y-residuals averaged by night.

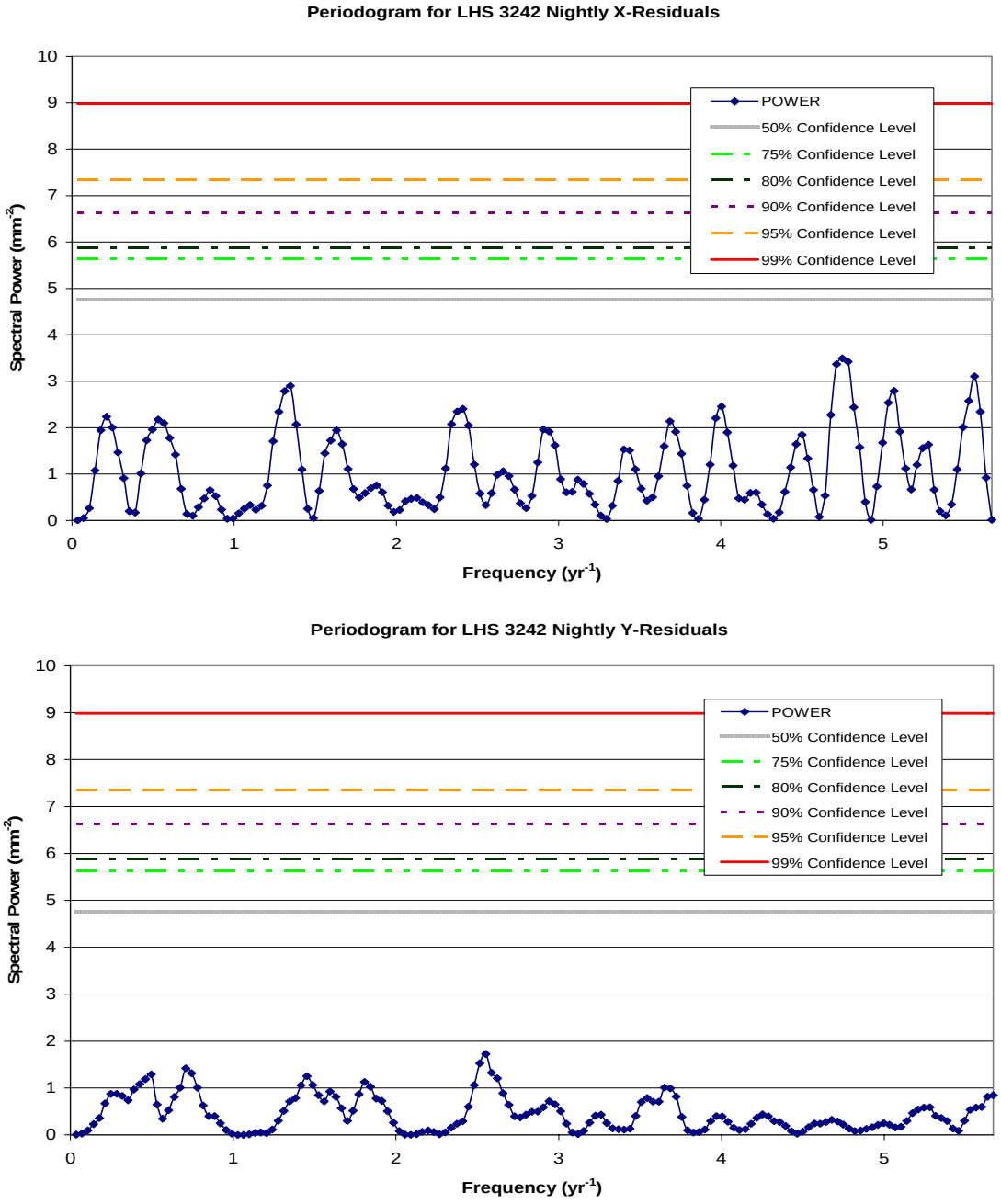

FIG. 3.28.—LHS 3242 Periodograms. Top chart is a periodogram calculated for nightly x-residuals. Bottom chart is a periodogram calculated for nightly y-residuals. Horizontal lines in the periodograms indicate likelihood that spectral peaks exceeding that power are real and not caused by noise only. Solid line is 99% confidence, dashed line 95% confidence, dotted line 90% confidence, dash dotted line is 80% confidence, dash double-dotted line is 75% confidence, and hashed line is 50% confidence.

TABLE 3.24
FEATURES OF PERIODOGRAMS FOR LHS 3242

Feature	Frequency (yr^{-1})	Period (yr)	Power (mm^{-2})	False Alarm Probability (%)	Comment
All X, maximum	6.2	0.16	8.1	15	frequency too high for nightly residuals
All Y, maximum	33.6	0.03	14.7	<1	frequency too high for nightly residuals
Nightly X, maximum	4.8	0.21	3.5	92	
Nightly Y, maximum	2.6	0.39	1.7	>99	

3.2.2.13 LHS 3418

LHS 3418 is approximately 22 pc away (BIP), slightly closer than the other M3.5 V (Hawley, Gizis, & Reid 1996) star in this study, LHS 2739. LHS 3418 also ties LHS 2739 for the smallest error associated with the calculation of its relative parallax. Its mean error of unit weight in y is also the smallest. The quality of the parallax and proper motion solution along with its moderate baseline contributed to the inclusion of LHS 3418 in the second subsample. LHS 3418 and its reference stars were all corrected for DCR.

The residuals displayed in Figure 3.29 and analyzed in Figure 3.30 do not indicate the presence of any companions. A limit to the size of any companions missed by this study is set in section 3.2.3 at $17 \pm 2\ M_{2l}$. The maxima in the nightly x- and nightly y-residuals occur at adjacent frequencies, 5.20 yr^{-1} and 5.23 yr^{-1} respectively, which correspond to periods of approximately 70 days, but both have high false alarm probabilities. The corresponding points in periodograms for all residuals have a greater than 50% chance of being real and are adjacent to local peaks. The distribution of observations makes periods less than one year highly unlikely. The maxima for the both periodograms for all residuals occur at frequencies too high to appear in the nightly periodograms. Table 3.25 summarizes the features discussed.

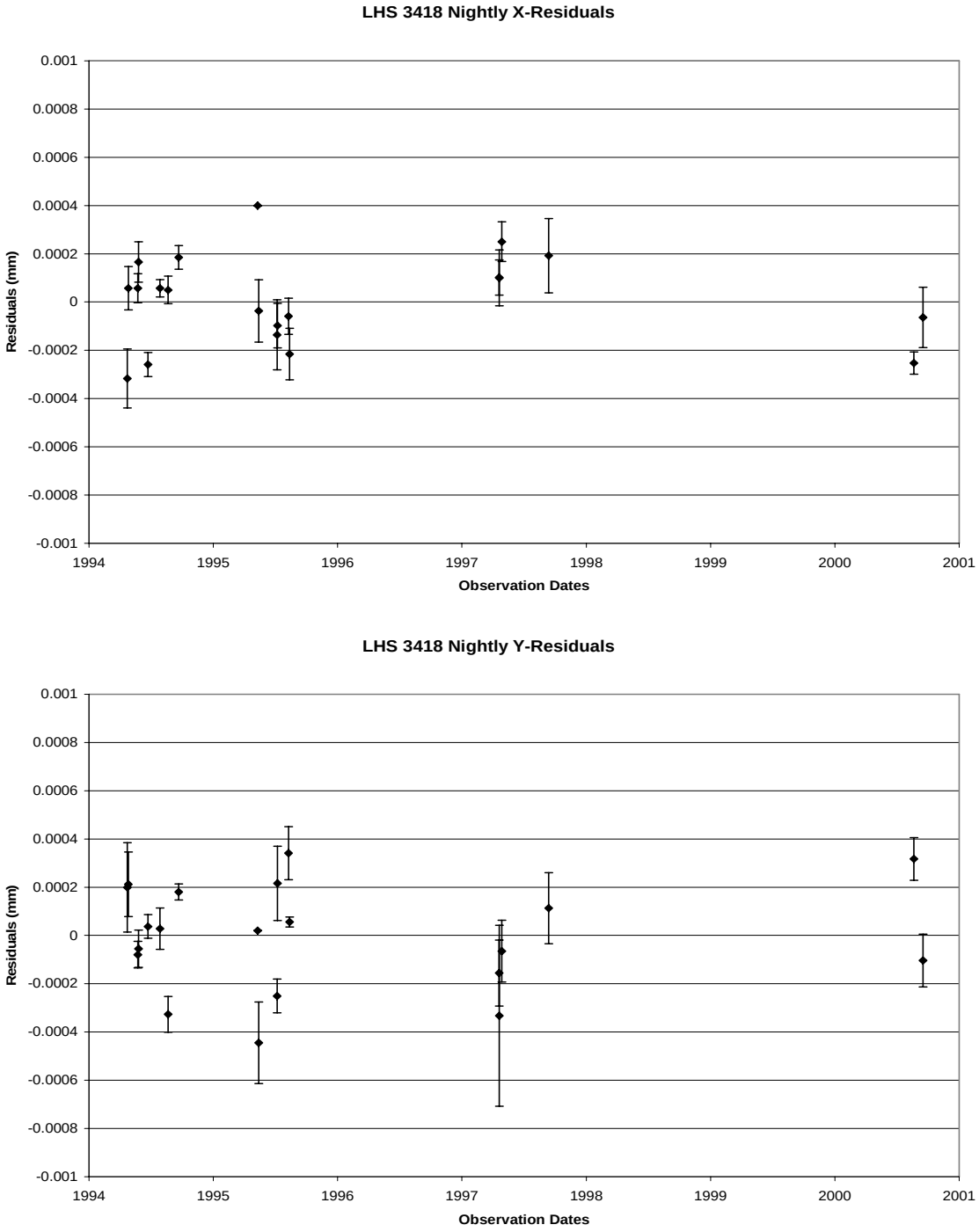

FIG. 3.29.—Nightly X- and Y-Residuals for LHS 3418. Top chart contains x-residuals averaged by night. Bottom chart contains y-residuals averaged by night.

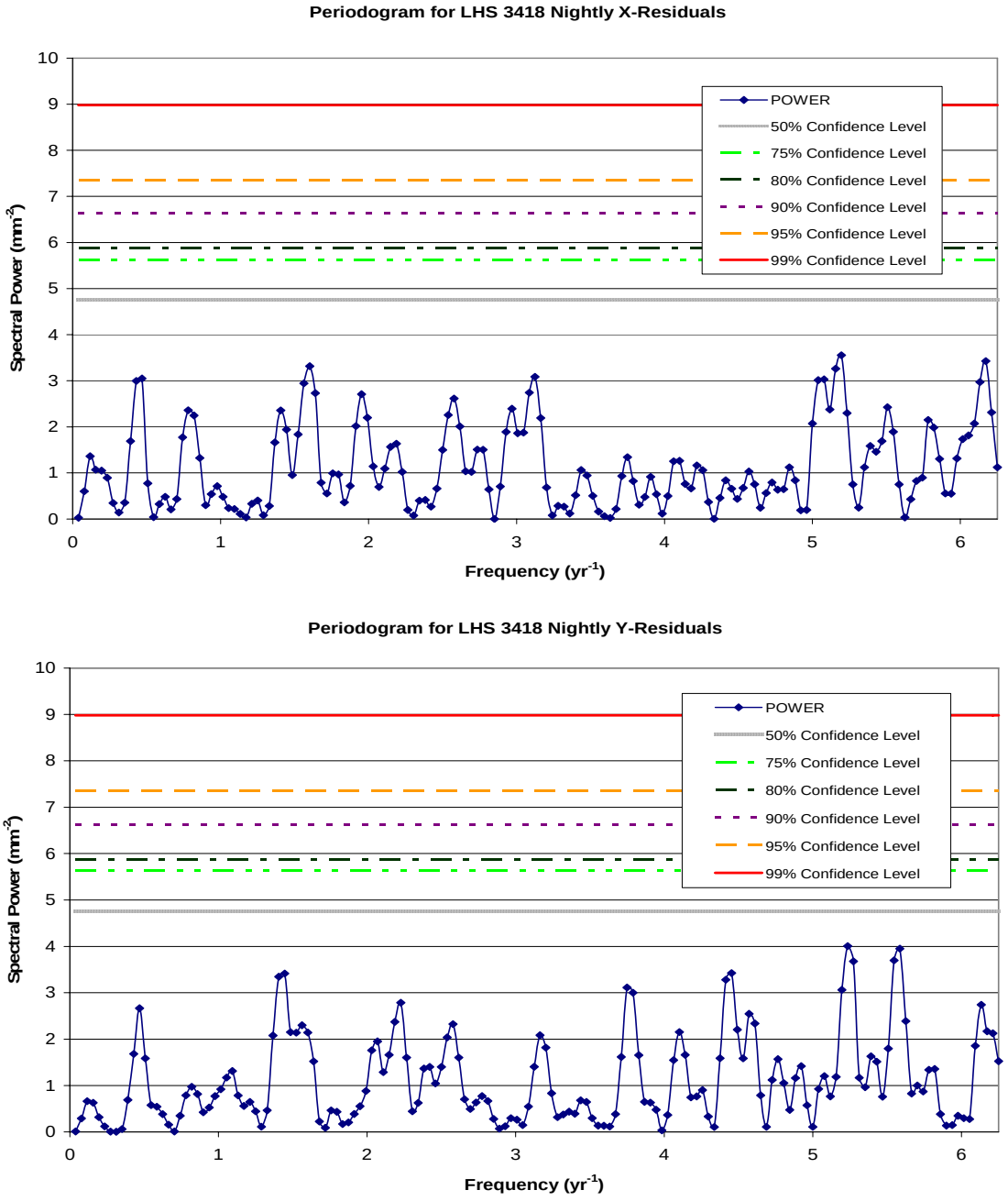

FIG. 3.30.—LHS 3418 Periodograms. Top chart is a periodogram calculated for nightly x-residuals. Bottom chart is a periodogram calculated for nightly y-residuals. Horizontal lines in the periodograms indicate likelihood that spectral peaks exceeding that power are real and not caused by noise only. Solid line is 99% confidence, dashed line 95% confidence, dotted line 90% confidence, dash dotted line is 80% confidence, dash double-dotted line is 75% confidence, and hashed line is 50% confidence.

TABLE 3.25
FEATURES OF PERIODOGRAMS FOR LHS 3418

Feature	Frequency (yr^{-1})	Period (yr)	Power (mm^{-2})	False Alarm Probability (%)	Comment
All X, maximum	30.038	0.033291	14.240	<1	frequency too high for nightly residuals
All X, local peak	5.1561	0.19394	8.7494	<10	adjacent to frequency of interest
All X, adjacent to local peak	5.1952	0.19249	8.6350	<10	corresponds to maximum in nightly x
All X	5.2343	0.19105	5.3922	>50	correspond to maximum in nightly y
All Y, maximum	6.7967	0.14713	12.424	<1	frequency too high for nightly residuals
All Y, local peak	5.2733	0.18963	9.4221	<5	adjacent to frequency of interest
All Y, adjacent to local peak	5.2343	0.19105	8.5760	<10	corresponds to maximum in nightly y
All Y	5.1952	0.19249	5.9664	>50	corresponds to maximum in nightly x
Nightly X, maximum	5.195	0.1925	3.553	90	adjacent to maximum in nightly y
Nightly X, adjacent to maximum	5.234	0.1910	2.297	>50	corresponds to maximum in nightly y
Nightly Y, maximum	5.234	0.1910	4.007	77	adjacent to maximum in nightly x
Nightly Y, adjacent to maximum	5.195	0.1925	3.063	>50	corresponds to maximum in nightly x

3.2.3 Companion Mass Limits

Despite expectations to find at least one substellar companion amongst the stars observed by the CCD extension of the SPP, no such unseen body was clearly detected. Because the numbers of extrasolar planets found to date remains small, non-detections contribute to the understanding of planetary frequency. Therefore, the sensitivity of this study to planets must be established. Assuming a circular orbit for simplicity, Kepler's third law estimates the minimum detectable companion mass (M_p)

$$M_p = \left(\frac{M_*}{P} \right)^{\frac{2}{3}} \frac{\alpha}{\pi} \tag{3.5}$$

where M_* is the stellar mass in solar mass units ($M_\odot$), P is the period in years, π is the absolute parallax in milliseconds of arc (mas), and α is the minimum detectable perturbation in mas.

Known binary systems were excluded from this study so the masses of potential host stars must be estimated from an appropriate mass-radius relationship or mass-luminosity relationship. The former applies only to LHS 34, the sole white dwarf in this study. Bergeron, Leggett, and Ruiz (2001) obtained a mass of $0.72 \pm 0.06\ M_\odot$ for this stellar remnant. Through astrophysical modeling, they obtained the effective temperature and the solid angle. Using an absolute parallax of 141.2 ± 8.4 mas (van Altena, Lee, & Hoffleit 1995), they converted the solid angle to a radius, which they fit to their cooling sequences to determine the mass. Because their radius assumes LHS 34 is nearer than indicated by the SPP relative parallax of 117.9 ± 1.8 (BIP), their mass may be considered an upper limit. The calculated radius of LHS 34 will increase with

estimated distance and, for white dwarfs, larger radii correspond to smaller masses. Although when corrected to an absolute parallax the SPP value will increase, it will remain smaller than 141 mas.

The majority of the stars in this study are M dwarfs so Table 3.26 lists mass estimates based on the K-band relationship derived by Delfosse *et al*. (2000). Their mass-luminosity relationship is based on the hybrid photometric system described by Leggett (1992), who adopted California Institute of Technology infrared colors defined by Elias *et al*. (1982, hereafter CIT). J (1.235 μm) and K_S (2.16 μm) photometry from the Two Micron All Sky Survey (Skrutskie *et al*. 2006, hereafter 2MASS; Cohen, Wheaton, and Megeath 2003) was converted to K_{CIT} (2.2 μm). The absolute K_{CIT} magnitudes were estimated using the preliminary relative parallaxes in Table 3.5. These absolute magnitudes are upper limits. The eventual correction to absolute will increase the parallaxes slightly, which would produce a larger absolute magnitude. The absolute K_{CIT} magnitudes were then converted to stellar masses using the K-band mass-luminosity relationship (Delfosse *et al*. 2000). These masses are also upper limits; an increase in absolute luminosity will decrease the corresponding mass. Using absolute parallaxes can be expected to reduce the masses herein by less than 2.5%.

TABLE 3.26
STELLAR MASSES ESTIMATED FROM INFRARED PHOTOMETRY

Star (LHS)	2MASS J (mag)	2MASS K_S (mag)	CIT K (mag)	CIT M_K (mag)	Mass ($M_\odot$)	Comment
34	12.726 ± 0.023	12.362 ± 0.024	12.381 ± 0.024	12.738 ± 0.042	…	white dwarf
271	7.953 ± 0.024	7.037 ± 0.017	7.055 ± 0.018	7.990 ± 0.027	0.176 ± 0.043	
288	8.492 ± 0.021	7.728 ± 0.027	7.746 ± 0.028	9.392 ± 0.033	0.096 ± 0.043	
337	8.174 ± 0.024	7.386 ± 0.021	7.404 ± 0.022	8.225 ± 0.030	0.157 ± 0.043	
532	8.984 ± 0.026	8.108 ± 0.023	8.126 ± 0.024	7.996 ± 0.040	0.175 ± 0.043	
1134	8.572 ± 0.019	7.710 ± 0.016	7.728 ± 0.017	7.711 ± 0.052	0.201 ± 0.043	
1565	7.523 ± 0.020	6.610 ± 0.021	6.628 ± 0.022	8.899 ± 0.024	0.116 ± 0.043	
2310	9.052 ± 0.029	8.139 ± 0.023	8.157 ± 0.024	7.416 ± 0.092	0.233 ± 0.044	
2739	9.329 ± 0.029	8.517 ± 0.027	8.535 ± 0.028	6.733 ± 0.053	0.324 ± 0.043	
2813	8.926 ± 0.027	8.123 ± 0.024	8.141 ± 0.025	7.025 ± 0.068	0.282 ± 0.044	
3064	9.094 ± 0.024	8.274 ± 0.023	8.292 ± 0.024	7.880 ± 0.036	0.185 ± 0.043	
3242	8.04 ± 0.024	7.224 ± 0.020	7.242 ± 0.021	6.293 ± 0.049	0.397 ± 0.043	
3418	9.305 ± 0.020	8.457 ± 0.024	8.475 ± 0.025	6.751 ± 0.050	0.322 ± 0.043	

REFERENCES.—CIT K magnitudes calculated from listed 2MASS photometry in accordance with Carpenter 2006. Masses calculated from CIT M_K according to Delfosse *et al*. 2000.

The periods considered also affect the ability of a program to detect companions of various sizes. Ideally, the observations should be span more than a single orbit in order to adequately separate the companion-induced perturbation from the proper motion term (Black & Scargle 1982). Radial-velocity surveys are sensitive to short-period planets that produce a large velocity change in the host star. Astrometric techniques, however, are best suited to finding planets with longer orbital periods that produce largerdisplacements in the host star (Quirrenbach *et al*. 2004). The longest period considered for each stars is its observational baseline, listed in Table 3.8. A planet with a one-year period is likely to be missed because of confusion with the annual cycle associated with parallax observing. Therefore, the shortest period considered is 1.5 years in every case.

Setting the minimum detectable perturbation (α) is the most subjective step because of the quality and quantity of available data varies and because misleading peaks will appear in periodogram when a large number of frequencies are evaluated (Scargle 1982). Minimum detectable perturbations (α) of 10–20 mas have been suggested in literature (Campbell, Walker, & Yang 1988; Heintz 1988) and are discussed in Chapter 2. Chapter 2 indicates a slightly larger minimum detectable perturbation of 21.3 ± 3.5 mas for photographic plates taken with the Leander McCormick Observatory (McCormick) 26.25-inch (67-centimeter) refractor, which has a plate scale of about 20,750 mas millimeter^{-1}. Expressed in micrometers, the perturbation would be 1.03 ± 0.17 μm, which is a little less than the size of the average residual, which was 1.12 ± 0.89 μm.

The digital images available from CCD's may be measured more precisely than photographic plates measured on a microdensitometer. Positions on a CCD image may be repeatable to about one-fiftieth (~0.02) of a pixel (Monet *et al*. 1992), which translates to 0.44–0.45 micrometer (μm) or 11.2–11.5 milliseconds seconds of arc (mas) for the Siding Spring Observatory 1-meter reflector. The CCD's and telescope used by the SPP may be considered typical of such programs; the best endeavors may achieve positions better than 0.3 μm (Monet *et al*. 1992). In comparison, positions of McCormick photographic plates were measured by the Photometric Data Systems (PDS) 1010GM Microdensitometer with an accuracy of about 1.5 μm, which translates to 31 mas for that telescope. Consequently, the average residuals for the SPP planet search were less than 0.5 μm, less than 0.4 μm for nightly normal points, while the average residual for the Barnard's Star study was over 1 μm, or about 0.6 μm for nightly normal points. Therefore, the SPP will be more sensitive to smaller perturbations. Assuming a similar ratio of minimum detectable perturbations to average residuals, Table 3.27 provides estimates of the minimum detectable perturbation for each potential host, which range from 5.4 to 10 mas.

TABLE 3.27
MINIMUM DETECTABLE PERTURBATIONS FOR POTENTIAL HOST STARS

Star (LHS)	Average Residual (μm)	Alpha (μm)	Alpha (mas)
34	0.30 ± 0.23	0.27 ± 0.31	7.0 ± 7.8
271	0.44 ± 0.40	0.40 ± 0.49	10 ± 13
288	0.36 ± 0.28	0.33 ± 0.37	8.4 ± 9.6
337	0.29 ± 0.24	0.26 ± 0.31	6.7 ± 7.9
532	0.29 ± 0.21	0.26 ± 0.29	6.7 ± 7.4
1134	0.29 ± 0.22	0.26 ± 0.30	6.7 ± 7.6
1565	0.28 ± 0.25	0.26 ± 0.31	6.7 ± 8.0
2310	0.43 ± 0.36	0.39 ± 0.46	10 ± 12
2739	0.24 ± 0.19	0.22 ± 0.25	5.6 ± 6.3
2813	0.39 ± 0.30	0.36 ± 0.40	9 ± 10
3064	0.27 ± 0.21	0.25 ± 0.27	6.3 ± 7.0
3242	0.32 ± 0.27	0.29 ± 0.34	7.5 ± 8.8
3418	0.23 ± 0.19	0.21 ± 0.24	5.4 ± 6.3

Finally, the parallax used in calculating the minimum mass of a detectable planet should ideally be the absolute parallax. However, absolute parallaxes are not yet available for the SPP so the preliminary relative parallaxes from Table 3.5 are used with the understanding that the correction to absolute will increase the parallax values slightly. Typical corrections to absolute are on the order of 1 mas, which would bring these stars up to about 2.3% nearer, so the lack of such correction has a minimal effect.

3.2.3.1 Limits for the Sample Generally

With values for each of the terms in Equation 3.5, the minimum detectable companion mass may be calculated. Table 3.28 lists the minimum detectable masses for short and long periods detectable for each potential host star. For low mass stars, such as those studied herein, the detection of a companion of any size would be significant. Additional nearby low-mass binaries would help define the mass-luminosity

relationship for the lower main sequence and provide constraints on formation theories for brown dwarfs and planets (Delfosse *et al*. 2000; Henry 2004).

TABLE 3.28
MINIMUM DETECTABLE COMPANION MASSES FOR POTENTIAL HOST STARS

Star (LHS)	Short Period ($M_{2\downarrow}$)			Longest Period ($M_{2\downarrow}$)			Comment
34	38.1	±	2.2	13.84	±	0.80	sensitive to brown dwarfs
271	16.8	±	2.7	4.75	±	0.77	
288	6.6	±	2.0	2.42	±	0.72	sensitive to planets
337	10.7	±	1.9	6.3	±	1.1	sensitive to planets
532	17.9	±	2.9	6.3	±	1.0	
1134	18.6	±	2.7	7.4	±	1.1	
1565	4.5	±	1.1	1.72	±	0.42	sensitive to planets
2310	42.8	±	5.6	15.8	±	2.1	sensitive to brown dwarfs
2739	48.0	±	4.4	17.0	±	1.5	sensitive to brown dwarfs
2813	52.1	±	5.6	16.9	±	1.8	sensitive to brown dwarfs
3064	19.6	±	3.0	6.4	±	1.0	
3242	50.0	±	3.8	17.8	±	1.3	sensitive to brown dwarfs
3418	44.5	±	4.1	16.9	±	1.6	sensitive to brown dwarfs

NOTE.—Short period is 1.5 years for all stars. The longest period is equal to the observational baseline listed in Table 3.8.

For short period orbits, the SPP is only capable of detecting planets around LHS 288, LHS 337, and LHS 1565. For the other stars, the minimum detectable mass is greater than 13 $M_{2\downarrow}$, which is the current upper mass limit set by the IAU WG ESP for a planet; planets should not have enough mass to support thermonuclear fusion of deuterium.[10] Even for periods as long their observational baseline, nearly half the sample remains insensitive to planetary perturbations. In most cases, brown dwarfs with periods of a few years may be ruled out as companions to these stars. In addition, these

[10]The IAU WG ESP provides their current definition of planet at http://www.dtm.ciw.edu/boss/definition.html

periods correspond to separations smaller than 4 AU. Planets, especially moderate gas giants and smaller, may still be present.

Again, the correction of the relative parallaxes used herein to absolute parallaxes will slightly reduce the minimum detectable masses through the direct application of parallax and, for the red dwarfs, through its effect on the estimation of stellar masses. Assuming a typical correction of about 1 mas, the minimum detectable masses will reduced by less than 4%, or no more than 2 $M_{\odot}$, which does not significantly improve the SPP detection capability.

3.2.3.2 Limits for LHS 288

This study identified potential astrometric signals with periods of approximately 3.4 and 6.8 years in the final periodograms calculated for LHS 288. Figure 3.1 includes estimates of the perturbation for LHS 288 due to brown dwarfs. Although these strong peaks do not establish the presence of an unseen companion, the mass associated with any such hypothetical companion is worth considering. The minimum detectable perturbation estimated for LHS 288 above was based on the size of residuals in the final analysis of the SPP data. Therefore, it can also be taken as the size of the perturbation detected if either the 3.4- or 6.8-year period is real. The latter period is the same as the observational baseline. As shown in Table 3.29, these periods correspond to planets with masses of 2–7 $M_{\odot}$. Such planets would lie within about 2 AU. Assuming the correction to absolute for LHS 288 is about 1 mas, the minimum detectable mass would decrease by less than 1%. A planet with a mass similar to Jupiter in a 1.5-year orbit

would produce a displacement of about 1.3 mas, which is well below the SPP sensitivity threshold.

TABLE 3.29
POTENTIAL MASSES FOR LHS 288 COMPANIONS CORRESPONDING TO DIFFERENT PERIODS

Period (years)	Companion Mass (M_{2l})	Comment
1.5 …	6.6 ± 2.0	shortest period considered
3.39 ± .48	3.8 ± 1.2	corresponds to x-periodogram maxima
6.8 ± 1.8	2.42 ± 0.84	baseline, corresponds to y-periodogram maxima

Leinert *et al*. (1997) used K-band speckle interferometry to search for companions orbiting LHS 288. They set lower limits for the absolute K magnitude of possible companions at various orbital distances, which are listed in Table 3.30 on the following page. They based their absolute magnitudes on an absolute parallax of 220 ± 10 mas from the *Preliminary Version of the Third Catalogue of Nearby Stars* (Gliese & Jahreiß 1991). From these magnitude limits, corresponding masses and periods were calculated. First, the absolute K magnitudes were adjusted to the SPP parallax of 213.4 ± 1.7 mas for consistency with other LHS 288 estimates. The magnitudes in Table 3.30 are too large for the K-band mass-luminosity relationship used elsewhere in this study (Delfosse *et al*. 2000) and for the relationships from related speckle interferometric studies (Henry & McCarthy 1993). Therefore, masses were estimated using an earlier

TABLE 3.30
COMPANION MASS LIMITS FOR LHS 288 FROM SPECKLE INTERFEROMETRY

Distance (AU)	M_K (mag)	Mass ($M_{\odot}$)	Period (years)	Comment
1	11.6	35.0 ± 2.2	2.8 ± 2.1	brown dwarf, short period
2	12.1	28.2 ± 1.8	8.1 ± 9.1	brown dwarf, period longer than baseline
5	13.4	16.1 ± 1.0	34 ± 25	
10	14.1	11.87 ± 0.75	97 ± 73	planet, period much longer than baseline

REFERENCE.—Distance and absolute magnitude from Leinert *et al*. 1997

mass-luminosity relationship from a speckle interferometric study of northern-hemisphere red dwarfs (Henry & McCarthy 1990). Once companion masses were computed, corresponding periods were calculated using Kepler's third law. With periods accessible to SPP observations, their study would primarily have found brown dwarfs. The lowest mass to which they would have been sensitive is a planet with a mass of approximately 12 $M_{\odot}$ orbiting at 10 AU with a period of nearly 98 years. Although this mass is well above the minimum detectible companion masses found for LHS 288, the period far exceeds the observational baseline.

In addition, Jao *et al*. (2003) examined astrometric images of 209 stars taken as part of the CTIOPI for companions within 20" of the parallax star. For LHS 288, this separation translates to about 94 AU, which corresponds to a period of approximately 2,900 years. The R_C images of LHS 288 revealed no companions. Of the eight new multiples detected by this study, LTT 7419 AB had the largest magnitude difference, 6.1 magnitudes in V_{JM}. The new companions are all probably low-mass main sequence stars or white dwarfs. Their investigation is unlikely to have imaged gas giants.

If the periodograms for LHS 288 reflect the presence of physical companions, those bodies are too small to have been detected by the earlier investigations of this star. If the peaks are the result of noise, then this study further narrows the possibilities that LHS 288 hosts giant planets.

3.3 DISCUSSION

The failure to detect the clear signal of a companion of any kind in this selection of the SPP stars is disappointing; it may be an indication that gas giants are less common around M dwarfs than Sun-like stars. If the suggested perturbation of LHS 288 is not spurious, then the detection of a single planet in this sample is well within expectations. The detection of astrometric companions is biased towards large long-period orbits. Although the baselines available here are sufficient to determine adequate parallaxes, they do not appear to be adequate for planet detection; the average baseline is 6.9 ± 1.5 years. Another 2–6 years would bring the long-period perturbation sensitivity to planets around all the stars. More observations over the course of the SPP would have reduced the residuals and improved the sensitivity to lower mass companions. When the second subsample was selected, another nine stars were considered for inclusion but failed to meet the final criteria. Perhaps one of these harbors an unseen companion.